RESEARCH ARTICLE

Spectraplakin is required for dendritic microtubule organization via a tip-based mechanism in *Drosophila*

Matthew Davies[1], Neeraja Sanal[1], Neele Wolterhoff[1†], Ulrike Gigengack[1], Yitao Shen[2], Samuel M Frommeyer[1], Ines Hahn[3], Sebastian Rumpf[1]*

[1]Institute for Neurobiology, Multiscale Imaging Center, University of Münster, Röntgenstrasse, Münster, Germany; [2]Biochemistry and Molecular Biology and the Huck Institutes of the Life Sciences, The Pennsylvania State University, University Park, United States; [3]York Biomedical Research Institute, Department of Biology, University of York, York, United Kingdom

***For correspondence:** rumpfsebastian4@gmail.com

Present address: †Division of Neurobiology, Institute for Biology, Freie Universität Berlin, Berlin, Germany

Competing interest: The authors declare that no competing interests exist.

Funding: See page 22

Preprint posted 30 June 2025
Sent for Review 27 June 2025
Reviewed preprint v1 22 August 2025
Reviewed preprint v2 23 September 2026
Version of Record 05 November 2026

Reviewing Editor: Kassandra M Ori-McKenney, University of California, Davis, United States

© Copyright Davies *et al*. This article is distributed under the terms of the Creative Commons Attribution License, which permits unrestricted use and redistribution provided that the original author and source are credited.

eLife Assessment

Davies et al. present a **valuable** study proposing that the Drosophila homologue of MACF1, Shot, can act as a molecular linker between microtubules and actin during dendrite pruning, suggesting an intriguing role in non-centrosomal microtubule organization. The study provides robust evidence that Shot helps control microtubule organization and dendrite pruning, but the evidence that Shot coordinates these processes through its interaction with actin remains **incomplete**, particularly because the actin-disrupting experiment does not affect the distal dendrites where the authors propose Shot acts. Overall, the study contains several interesting findings, but additional experimental support is needed to establish how Shot, actin, and microtubules work together to control dendrite pruning.

Abstract The differential microtubule organization in axons and dendrites underlies neuronal polarity and developmental processes, like neurite pruning. How neurons achieve their specific microtubule organization during development is an area of active research, and it has been especially hard to explain how dendritic microtubules are oriented with their plus ends toward the soma. Transient microtubule nucleation from tips of early growing dendrites has been proposed as a mechanism that would explain how this orientation is set up. In a survey for cytoskeletal regulators involved in dendrite pruning and microtubule organization in *Drosophila*, we found the spectraplakin Short stop (Shot), an actin/microtubule crosslinker. Loss of Shot causes microtubule orientation defects already during early dendrite development, when Shot is transiently recruited to tips of growing dendrites via its actin-binding domain. Genetic and functional evidence suggests that Shot's primary function in this process is to locally stabilize microtubules. We also provide evidence for an independent, developmentally transient microtubule nucleation mechanism. Our data highlight the importance of transient and localized microtubule regulation for dendritic microtubule organization.

Introduction

Microtubules are long polar tube-like polymers composed of α/β-tubulin dimers that provide mechanical stability to cells and act as tracks for motor-based transport. Tubulin dimers are preferentially added, and also lost, at microtubule plus ends, whereas microtubule minus ends are relatively inert and often localize to microtubule organizing centers (MTOCs), structures of diverse composition that

nucleate or anchor microtubules. In dividing cells, the main MTOCs are centrosomes, but many non-dividing or differentiated cells have less well-characterized non-centrosomal (nc)MTOCs (**Akhmanova and Kapitein, 2022**).

Given their intrinsic polarity, microtubules, and the way they are organized in a given cell, play an important role in cellular polarity. This is particularly evident in neurons. In axons, all microtubules are oriented with their plus ends toward the distal synapses, thus enabling axon-specific transport, especially via kinesin-1. In contrast, a large fraction of dendritic microtubules is oriented with the plus ends toward the soma ('plus end-in'), enabling dendrite-specific transport via other motors including dynein. The plus end-in orientation is especially prevalent in invertebrates, where microtubules in primary dendrite branches are often almost uniformly plus end-in (**Rolls et al., 2007**). Despite the recognized importance of microtubule organization for neuronal function, it is still poorly understood how neuronal – and in particular, dendritic – microtubule organization is set up and maintained.

The differential organization of neuronal microtubules also underlies important neuronal morphogenetic processes. For example, the peripheral nociceptive class IV dendritic arborization (c4da) neurons of *Drosophila* larvae prune their long and branched sensory dendrites at the onset of metamorphosis. Pruning involves severing of proximal dendrite regions and subsequent degeneration of distal fragments (**Rumpf et al., 2017**; **Furusawa and Emoto, 2021**). The presumptive severing sites – located in primary or secondary dendrites – are marked by the local loss of microtubules, which predisposes them to mechanical tearing (**Krämer et al., 2023**). This local microtubule disassembly is initiated by an increase in microtubule dynamics at the onset of the pupal stage (**Herzmann et al., 2017**). Due to their uniform plus end-in orientation, the dendritic microtubules shrink from their plus ends in a coordinated fashion, eventually leading to the complete loss of microtubules in proximal dendrite regions (**Herzmann et al., 2018**; **Rumpf et al., 2019**). In support of this model, conditions that cause mixed orientation of dendritic microtubules either cause pruning defects or act as genetic enhancers of pruning mutants with microtubule-related functions. For example, the motor protein kinesin-2 together with its binding partner, the plus end-binder End-Binding protein 1 (EB1), guide polymerizing microtubules along preexisting ones, thus ensuring the maintenance of plus end-in orientation (**Mattie et al., 2010**). Loss of kinesin-2 causes pruning defects, while EB1 knockdown genetically enhances the pruning defects caused by the tau kinase Par-1 (**Herzmann et al., 2018**). Dendritic microtubule orientation and pruning defects are also caused by loss of the minus end binding protein Patronin (**Wang et al., 2019**) and the serine/threonine phosphatase PP2A (**Rui et al., 2020**; **Wolterhoff et al., 2020**). Loss of the microtubule polymerase Minispindles (Msps)/XMAP-215, an MTOC component, also causes defects in microtubule orientation (**Tang et al., 2020**), possibly linking dendritic microtubule orientation to microtubule nucleation.

While several factors are known to maintain uniform dendritic microtubule orientation in *Drosophila* peripheral neurons, it is not clear how dendritic microtubule orientation arises during development. One model for this has been put forward based on the *C. elegans* PVD neuron model system. Here, a ncMTOC residing on Rab11-positive recycling endosomes is localized at the tip of the outgrowing dendrite, and only the plus end-in microtubules emanating from this MTOC are maintained, thus promoting plus end-in orientation (**Liang et al., 2020**; **Harterink et al., 2018**). Whether tip-based mechanisms could also inform dendritic microtubule polarity in other systems is not known.

Spectraplakins are a family of actin/microtubule cytoskeletal crosslinker proteins with important roles in microtubule organization in differentiated cells (**Sanchez et al., 2021**; **Sun et al., 2019**; **Voelzmann et al., 2017**). Anchored to the cell cortex or other actin-rich structures via an N-terminal actin binding domain, they can tether microtubules via binding sites for the minus end binding protein Patronin (**Noordstra et al., 2016**; **Ning et al., 2016**; **Nashchekin et al., 2016**); furthermore, spectraplakins can recruit factors related to microtubule growth such as the plus end binder EB1 (**Slep et al., 2005**). Spectraplakins have important functions in the nervous system, as mutations in human Microtubule-Actin-Crosslinking Factor 1 (MACF1) cause severe brain malformations (**Dekker et al., 2025**), while neuron-specific MACF1 knockout of mouse leads to defects in neurite elaboration (**Ka and Kim, 2016**). Mechanistically, it was shown that the *Drosophila* spectraplakin Short stop (Shot) bundles and stabilizes microtubules in axons (**Alves-Silva et al., 2012**; **Okenve-Ramos et al., 2024**). This effect was mediated by its C-terminal GAS2 domain (**Okenve-Ramos et al., 2024**), a type of microtubule-binding domain known to bundle and sometimes even nucleate microtubules (**An et al., 2025**).

Here, we describe an important role for Shot in dendritic microtubule organization. Loss of Shot in c4da neurons causes mixed orientation of dendritic microtubules and consequently, dendrite pruning defects. We find that Shot is already required for uniform orientation during early dendrite growth stages, when it transiently localizes to dendrite tips in an actin-dependent manner. Domain analyses show that this actin-dependent localization is required for Shot's function. The GAS2 domain is also required, and Shot can increase dendritic microtubule density, indicating that it contributes to dendritic microtubule organization via a local stabilization mechanism. We also provide evidence that Rab11 is important for dendritic microtubule orientation and might be part of a transient dendritic MTOC. Our data suggest that tip-based mechanisms could be broadly involved in dendritic microtubule organization and identify Shot as an important player.

Results

Shot is required for c4da neuron dendrite pruning

The long and branched dendrites of third instar larval c4da neurons are completely pruned at the onset of the pupal stage, such that by 16 hours after puparium formation (h APF), they have lost all their dendrites (***Figure 1A, B, B'***). In order to identify new regulators of c4da neuron dendrite pruning, we expressed candidate RNAis in c4da neurons under *pickpocket (ppk)-GAL4* and assessed their effects at 16 h APF. This approach identified a dsRNA line targeting *Shot*, which encodes the sole *Drosophila* member of the spectraplakins, a family of large adaptor proteins with binding sites for actin and microtubules. C4da neurons expressing *shot* dsRNA had long and branched dendrites at the larval stage (***Figure 1C***), even though their dendritic field coverage seemed somewhat reduced compared to control neurons. At 16 h APF, dendrites could still be seen attached to the soma in almost half the c4da neurons expressing *shot* dsRNA (***Figure 1C' , H–J***), indicative of pruning defects. In order to confirm this result, we used Mosaic Analysis with a Repressible Cell Marker (MARCM) to generate c4da neuron clones homozygous for the loss-of-function allele $shot^3$ (***Kolodziej et al., 1995***). $shot^3$ mutant c4da neurons had shorter dendrites at the third instar stage compared to control MARCM c4da neuron clones (***Figure 1D, E***). At 16 h APF, most $shot^3$ mutant neurons still had dendrites attached to the soma (***Figure 1D', E', H–J***). We also generated an sgRNA line targeting an exon common to all Shot splice isoforms and found that it caused significant c4da neuron dendrite pruning defects when expressed in c4da neurons in a sensitized $shot^3$/+heterozygous background (***Figure 1F', G', H–J***).

C4da neurons undergo extensive remodeling during the pupal stage. Concomitantly with their dendrites, they also prune their presynapses in an ecdysone- and actin-dependent manner (***Furusawa et al., 2023***; ***Frommeyer et al., 2026***). Later during the pupal stage, c4da neurons grow new dendrites adapted to the adult stage, which requires cytoskeletal factors (***Kuo et al., 2005***; ***Yoong et al., 2020***; ***Sanal et al., 2023***). While Shot was not required for presynapse pruning (***Figure 1***, ***Figure 1—figure supplement 1C–E***), c4da neurons lacking Shot also failed to initiate dendrite regrowth at 72 h APF, when control c4da neurons had regrown long and branched dendrites (***Figure 1***, ***Figure 1—figure supplement 1C–E***). We conclude that Shot is required for c4da neuron dendrite remodeling, but does not seem to affect synapses.

Shot is required for uniform dendritic microtubule orientation

We and others have previously shown that c4da neuron dendrite pruning depends on local microtubule disassembly in proximal dendrites (***Williams and Truman, 2005***; ***Herzmann et al., 2017***; ***Herzmann et al., 2018***; ***Wang et al., 2019***). To assess a potential effect of Shot knockdown on dendritic microtubule regulation during the early pupal stage, we visualized dendritic microtubules at 6 h APF using immunofluorescence against the microtubule-associated protein futsch/MAP1B. While control neurons consistently showed gaps in their futsch signal in these regions (***Figure 2A and C***), Shot knockdown neurons often still displayed continuous futsch staining in their proximal dendrites (***Figure 2B, C***).

As microtubules shrink away from the cell body in a coordinated fashion during dendrite pruning, the uniform plus end-in orientation of dendritic microtubules is particularly important for dendritic microtubule disassembly (***Herzmann et al., 2018***; ***Rumpf et al., 2019***). To assess whether loss of Shot affects dendritic microtubule orientation, we expressed EB1::GFP in c4da neurons and live imaged it in primary and secondary dendrites. EB1 binds to the plus ends of growing microtubules (both

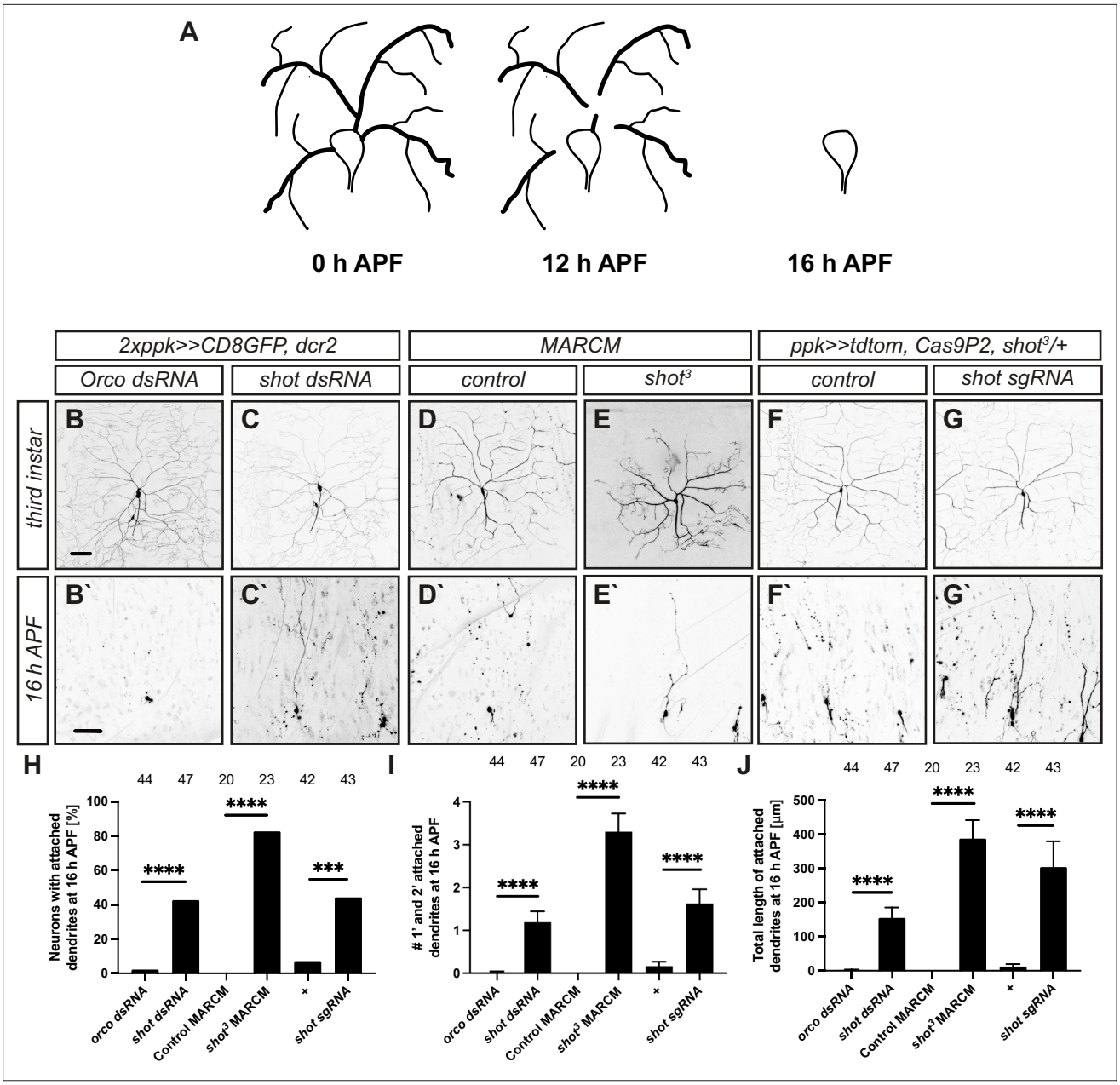


Figure 1. Shot is required for c4da neuron developmental dendrite pruning. (**A**) Schematic showing the progression of c4da neuron dendrite pruning via hormonal induction (0 h APF) to severing (12 h APF) and clearance (16 h APF). (**B–G'**) C4da neurons of the indicated genotypes were imaged at the third instar larval stage (**B–G**) and at 16 hours after puparium formation (h APF) (**B'–G'**). (**B**, **B'**) Control c4da neurons expressing Orco dsRNA under the control of *ppk-GAL4*. (**C**, **C'**) C4da neurons expressing Shot dsRNA under the control of *ppk-GAL4*. (**D**, **D'**) Control c4da neurons labeled by MARCM. (**E**, **E'**) *shot*^{3} mutant c4da neurons labeled by MARCM. (**F**, **F'**) Control c4da neurons expressing Cas9P2 under *ppk-GAL4* in a *shot*^{3} heterozygous background. (**G**, **G'**) C4da neurons coexpressing Cas9P2 and Shot sgRNA under the control of *ppk-GAL4* in a *shot*^{3} heterozygous background. (**H**) Phenotypic penetrance of pruning defects in (**B'–G'**). Number of neurons for each sample are indicated above the graph. ***p < 0.001, ****p < 0.0001, two-tailed Fisher's exact test. (**I**) Average number of primary and secondary dendrites attached to the soma at 16 h APF in samples (**B'–G'**). Values are mean ± SEM, ****p < 0.0001, Mann–Whitney *U* test. (**J**) Total length of remaining dendrites at 16 h APF in samples (**B'–G'**). Values are mean ± SEM, ****p < 0.0001, Mann–Whitney *U* test. Scale bars in (**B**) and (**B'**) are 50 µm.

The online version of this article includes the following figure supplement(s) for figure 1:

Figure supplement 1. Effect of microtubule regulators on c4da neuron synapse pruning and dendrite regrowth.

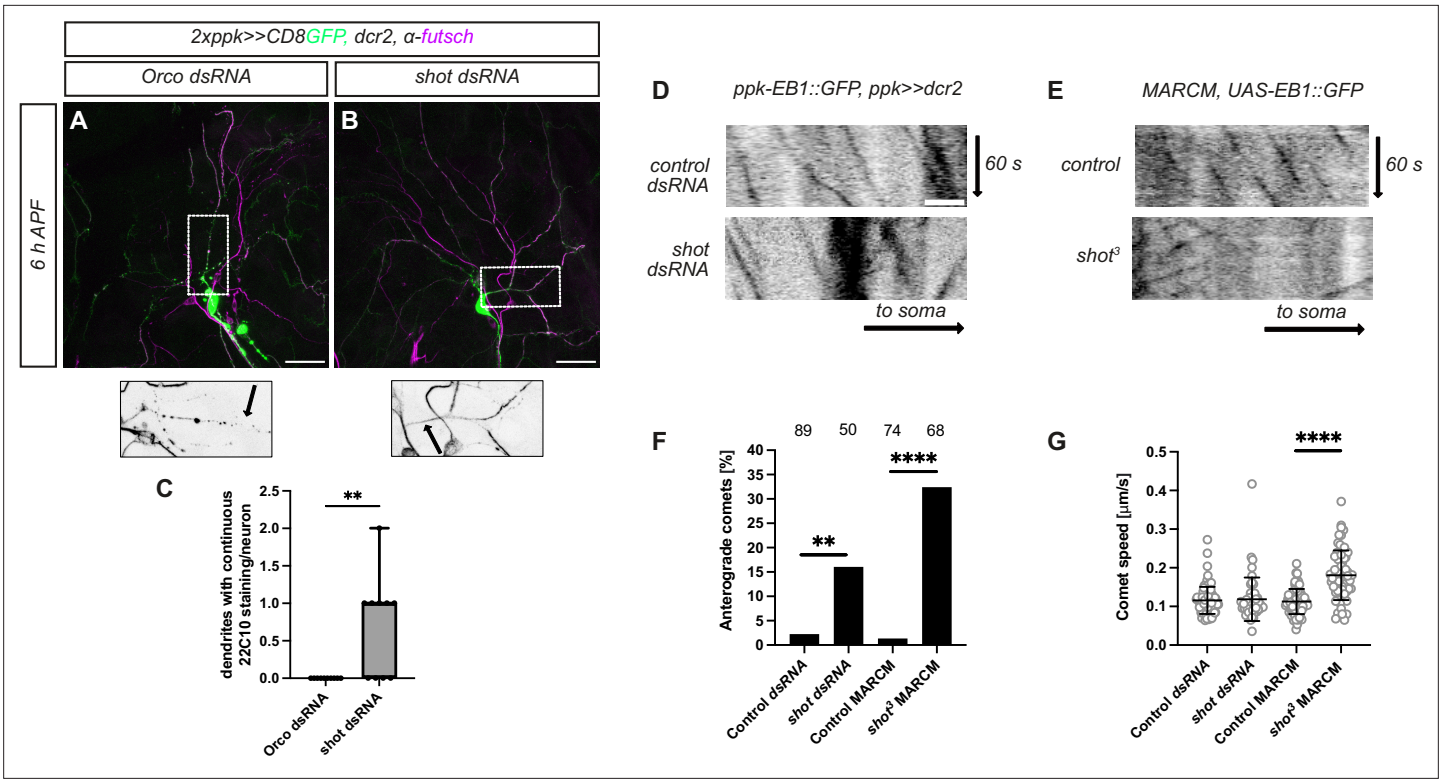


Figure 2. Shot is required for uniform plus end-in orientation of dendritic microtubules. (**A–C**) Delayed microtubule disassembly in neurons lacking Shot. Microtubules in control or Shot knockdown c4da neurons (green) were visualized by futsch/22C10 staining (magenta) at 6 h APF. Smaller panels below show futsch/22C10 signal in boxed areas in (**A**) and (**B**), arrows indicate c4da neuron dendrites. (**A**) Control c4da neuron. (**B**) C4da neuron expressing Shot dsRNA. (**C**) Graph depicting the average number of dendrites with continuous futsch/22C10 staining per neuron in (**A**) and (**B**). Box represents SD, *N* = 10 neurons each, **p < 0.01, Student's *t*-test. (**D**, **E**) EB1::GFP comets were imaged in primary dendrites of third instar larval c4da neurons, and comet movement was depicted in kymographs. Time and direction of the soma are indicated by arrows. (**D**) Upper panel, EB1::GFP comets in control neuron expressing Orco dsRNA; lower panel, EB1::GFP comets in neuron expressing Shot dsRNA. (**E**) Upper panel, EB1::GFP comets in control c4da neuron MARCM clone; lower panel, EB1::GFP comets in *shot*^{3} mutant c4da neuron MARCM clone. (**F**) Percentage of anterogradely moving comets in panels (**D**) and (**E**). Numbers of comets per sample are indicated above the graph (4, 15, 21, and 11 neurons, respectively, range 0–60% anterograde per neuron). **p < 0.01, ****p < 0.0001, two-tailed Fisher's exact test. (**G**) EB1::GFP comet speed in panels (**D**) and (**E**). ****p < 0.0001, Wilcoxon's test. Scale bars in (**A**) and (**D**) are 20 and 5 µm, respectively.

newly nucleated and re-elongating), and plus end-bound EB1 is visible as moving dots (also known as comets). The movement direction of EB1 comets then indicates the orientation of the respective microtubule. As expected, EB1::GFP comets in primary or secondary dendrites of third instar control c4da neurons moved exclusively retrogradely toward the soma, indicating plus end-in orientation (***Figure 2D, F***). Upon *shot* knockdown, a significant proportion of EB1::GFP comets (16%) could be seen moving anterogradely, or plus end-out (***Figure 2D, F***). To confirm this result, we assessed EB1::GFP behavior in control and *shot*^{3} c4da neuron MARCM clones and observed an even higher proportion (32%) of plus end-out dendritic microtubules in the mutant (***Figure 2E, F***). Comets in *shot*^{3} mutant neurons also moved at a slightly higher speed than in control neurons (***Figure 2G***). We conclude that Shot is required for the correct orientation of dendritic microtubules.

Actin and microtubule binding by Shot are crucial for pruning and microtubule organization

In order to better understand the function of Shot in dendritic pruning and microtubule orientation, we next asked which domains of Shot are crucial for these functions. Of particular interest were the domains of Shot that bind to actin and microtubules. Shot has two Calponin Homology (CH) domains at the N-terminus that mediate binding to specific actin structures, and a microtubule-binding GAS2 domain in its C-terminal region (***Figure 3A***). We next expressed full length or truncated Shot variants in *shot*^{3} mutant c4da neurons and asked whether they could rescue the pruning and microtubule

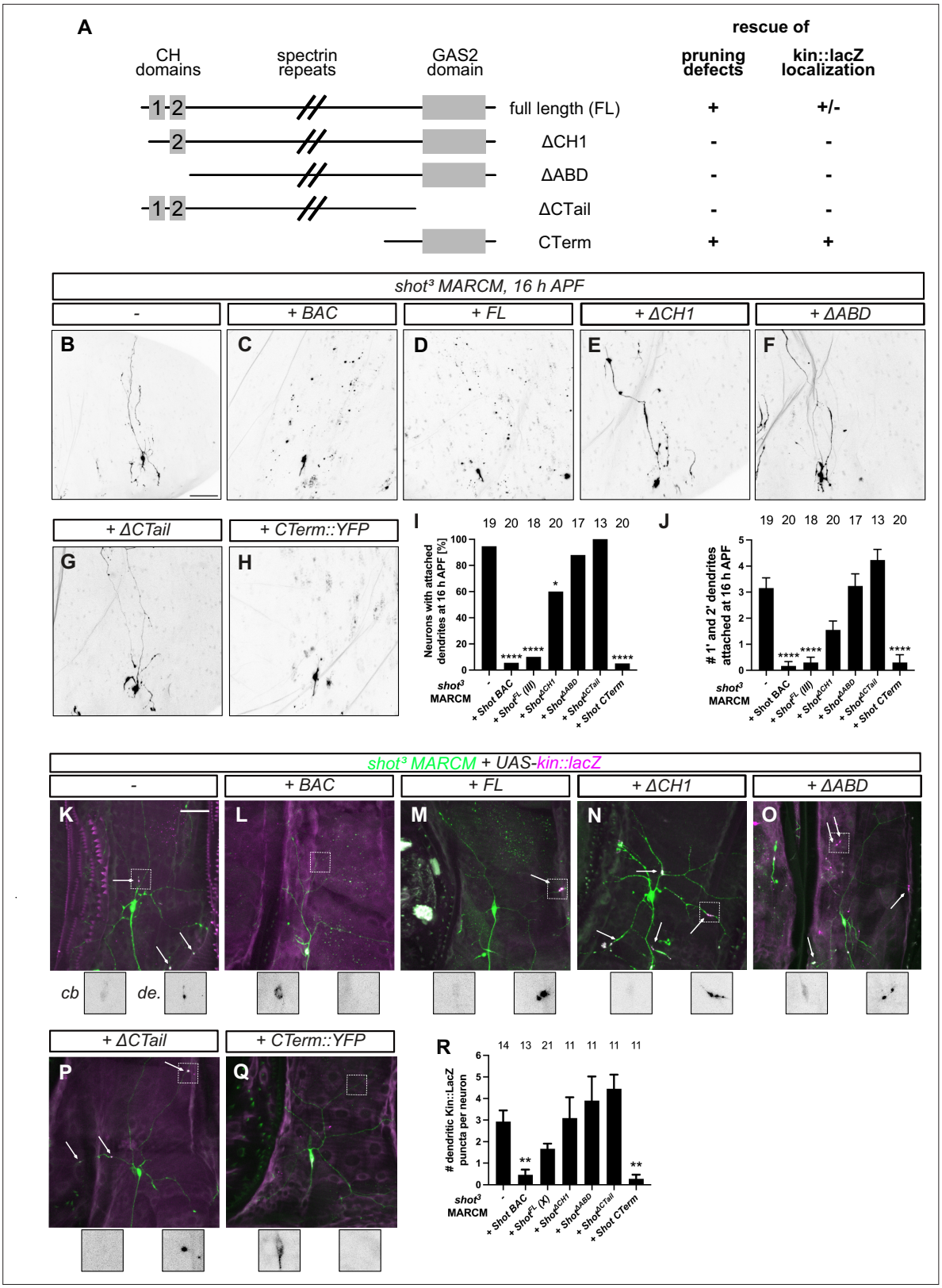


Figure 3. Shot domains important for pruning and microtubule organization. (**A**) Schematic of Shot domain structure and used UAS-Shot constructs. Right, summary of the phenotypic characterization below. CH, Calponin homology. (**B–J**) Ability of the indicated Shot UAS constructs to rescue the pruning defects of *shot*^{3} mutant c4da neuron MARCM clones at 16 h APF. (**B**) *shot*^{3} mutant c4da neuron. (**C**) *shot*^{3} mutant c4da neuron rescued by a genomic Shot::YFP BAC construct. (**D**) *shot*^{3} mutant c4da neuron expressing full-length Shot::GFP. (**E**) *shot*^{3} mutant c4da neuron expressing

Figure 3 continued on next page

Figure 3 continued

Shot$^{\Delta CH1}$::GFP. (**F**) *shot*^{3} mutant c4da neuron expressing Shot$^{\Delta ABD}$::GFP. (**G**) *shot*^{3} mutant c4da neuron expressing Shot$^{\Delta CTail}$::GFP. (**H**) *shot*^{3} mutant c4da neuron expressing Shot C-term::YFP. (**I**) Penetrance of pruning defects. Number of neurons per sample is indicated above the graph. *p < 0.05, ****p < 0.0001, two-tailed Fisher's exact test. (**G**) Number of primary and secondary dendrites attached to the cell body at 16 h APF. Values are mean ± SEM, ****p < 0.0001, Mann–Whitney *U* test. (**K–R**) Kin::lacZ localization in third instar *shot*^{3} c4da neuron MARCM clones. The insets below the panels show kin::lacZ signal in cell bodies (cb, left) and dendrites (den., right). (**K**) *shot*^{3} mutant c4da neuron. (**L**) *shot*^{3} mutant c4da neuron rescued by a genomic Shot::YFP BAC construct. (**M**) *shot*^{3} mutant c4da neuron expressing full-length Shot::GFP. (**N**) *shot*^{3} mutant c4da neuron expressing Shot$^{\Delta CH1}$::GFP. (**O**) *shot*^{3} mutant c4da neuron expressing Shot$^{\Delta ABD}$::GFP. (**P**) *shot*^{3} mutant c4da neuron expressing Shot$^{\Delta Ctail}$::GFP. (**Q**) *shot*^{3} mutant c4da neuron expressing Shot C-term::YFP. Asterisks in (**K–Q**) denote soma position, and arrows mark dendritic kin::lacZ puncta. (**R**) Number of dendritic kin::lacZ puncta in third instar c4da neurons expressing the indicated Shot UAS constructs. Number of neurons per sample is indicated above the graph. Values are mean ± SEM, **p < 0.01, Mann–Whitney *U* test. Scale bars in (**B**) and (**K**) are 50 µm.

The online version of this article includes the following figure supplement(s) for figure 3:

Figure supplement 1. Effect of Shot domain mutant overexpression on c4da neuron dendrite pruning.

orientation defects. We used a genomic Shot BAC rescue construct with a C-terminal YFP-tag and a UAS construct containing GFP-tagged full-length Shot UAS (Shot^{FL}::GFP) as full-length Shot variants. To address the role of the actin binding domain, we tested Shot$^{\Delta CH1}$::GFP, a Shot variant lacking the first CH domain with decreased affinity for actin (***Lee and Kolodziej, 2002***), and Shot$^{\Delta ABD}$::GFP, which lacks both CH domains. To address the function of microtubule binding, we either used a full-length Shot variant lacking the GAS2 domain (Shot$^{\Delta CTail}$::GFP), or Shot Cterm::YFP, a C-terminal Shot fragment containing only the GAS2 domain (***Figure 3A***). Of the above constructs, we noticed that Shot$^{\Delta CH1}$::GFP, but not the others, caused pruning defects when overexpressed under two copies of the c4da neuron driver *ppk-GAL4* (***Figure 3—figure supplement 1***).

Both the genomic Shot BAC construct and UAS-Shot^{FL}::GFP rescued the pruning defects of *shot*^{3} mutant neurons (***Figure 3B–D, I, J***). We next tested the domain mutants and found that while Shot$^{\Delta CH1}$::GFP slightly reduced the pruning defects of the mutant (***Figure 3E, I, J***), Shot$^{\Delta ABD}$::GFP and Shot$^{\Delta CTail}$::GFP could not rescue them at all (***Figure 3F, G, I, J***). Strikingly, expression of Shot Cterm::YFP containing only the GAS2 domain led to a full rescue of the pruning defects (***Figure 3H–J***).

We next asked whether these domains are also important for Shot's function in dendritic microtubule orientation. As the GFP tags of the Shot transgenes and the tdtomato fluorophore used to label MARCM clones precluded the use of fluorescently tagged EB1 constructs, we used kinesin-lacZ (kin::lacZ), a fusion between the kinesin-1 motor domain and β-galactosidase. Because the kinesin motor domain migrates toward microtubule plus ends, this fusion protein will always move toward the soma in dendrites with normal plus end-in orientation and will thus show staining in the soma, but not dendrites. Consistent with the observation that loss of Shot causes microtubule orientation defects, kin::lacZ was depleted from the soma and found in dendritic puncta in *shot*^{3} mutant c4da neurons (***Figure 3K, R***), but in animals carrying the genomic Shot BAC, it was localized in the soma (***Figure 3L, R***). UAS-based expression of Shot^{FL}::GFP in mutant neurons did not fully rescue kin::lacZ localization but reduced the number of dendritic kin::lacZ puncta (***Figure 3M, R***). *shot*^{3} mutant c4da neurons expressing Shot$^{\Delta CH1}$::GFP, Shot$^{\Delta ABD}$::GFP, or Shot$^{\Delta CTail}$::GFP did not confer rescue effects and showed many dendritic kin::lacZ puncta comparable to *shot*^{3} mutant neurons (***Figure 3N–P, R***). Again, expression of Shot Cterm::YFP restored dendritic exclusion of kin::lacZ, and it could be seen in the soma (***Figure 3Q, R***).

Thus, in the context of full-length Shot, both its actin and microtubule binding activities are required for its roles in dendrite pruning and microtubule orientation, but the isolated GAS2 domain alone was sufficient to rescue Shot function. This is reminiscent of a previous study reporting that full-length Shot is in an autoinhibited state that can be relieved by actin binding (***Applewhite et al., 2013***). In support of the notion that microtubule orientation defects cause pruning defects, the pruning and microtubule orientation defects of *shot* mutant neurons go hand in hand in our domain analysis.

Shot cooperates with actin to promote microtubule orientation

To independently probe for a role for actin in dendritic microtubule organization, we sought to manipulate actin dynamics in vivo. As treatment with actin-depolymerizing drugs like latrunculin would likely be highly toxic to larvae, we considered Mical, a potent actin severing enzyme that breaks actin filaments by oxidizing actin on specific methionine residues (***Grintsevich et al., 2017***). Mical is highly

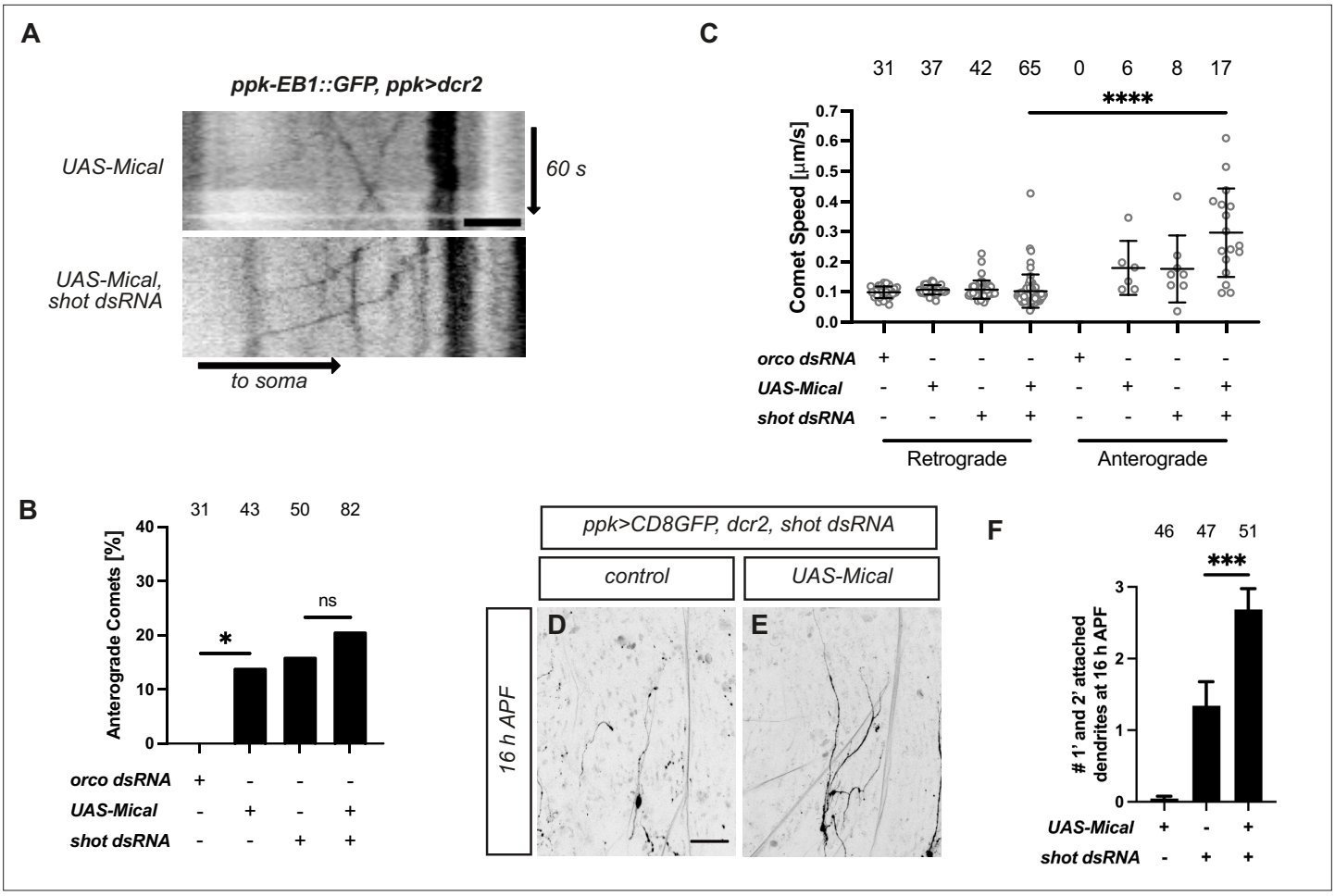


Figure 4. Shot and actin cooperatively regulate the behavior of dendritic microtubules. (**A**) Effect of actin severing on EB1::GFP comet movement. Mical was overexpressed in c4da neurons with or without Shot knockdown, and EB1 comets were analyzed as in ***Figure 2D***. Upper panel, kymograph of EB1 comet movement in c4da neuron overexpressing Mical. Lower panel, kymograph of EB1 comet movement upon Mical overexpression and *shot* knockdown. (**B**) Penetrance of anterograde dendritic EB1 comets in control c4da neuron expressing *orco* dsRNA, or in neurons expressing *shot* dsRNA, Mical, or both kymographs for the latter shown in (**A**). Number of comets per sample is given in the graph (9, 6, 15, and 14 neurons, respectively, range 0–62% anterograde per neuron). *p < 0.05, Fisher's exact test. (**C**) Speed of dendritic EB1 comets in (**A**) and (**B**). ****p < 0.0001, Wilcoxon's test. (**D–F**) Synergistic effects of Shot knockdown and Mical overexpression on c4da neuron dendrite pruning. (**D**) C4da neuron expressing shot dsRNA. and a control UAS construct at 16 h APF. (**E**) C4da neuron expressing shot dsRNA and UAS-Mical at 16 h APF. (**F**) Number of primary and secondary dendrites attached to the soma in c4da neurons overexpressing Mical, upon Shot knockdown, or both at 16 h APF. Number of neurons per sample is given in the graph. ***p < 0.001, Mann–Whitney *U* test. Scale bars are 5 µm in (**A**) and 50 µm in (**D**).

The online version of this article includes the following figure supplement(s) for figure 4:

Figure supplement 1. Effect of Mical overexpression on dendritic actin distribution.

specific for actin (***Rajan et al., 2023***) and its overexpression can disrupt actin bundles (***Hung et al., 2010***). Mical overexpression in larval c4da neurons did not grossly disrupt dendrite morphology, but altered F-actin distribution in that there was less seen in proximal dendrites at the first instar larval stage, as assessed by lifeact::GFP (***Figure 4—figure supplement 1***). We next tested whether Mical overexpression has an effect on dendritic microtubule orientation and found that it caused a significantly increased number of EB1::GFP comets in primary and secondary dendrites to move anterogradely (***Figure 4A, B***). When combined with Shot knockdown, Mical overexpression did not lead to an additive increase in the percentage of anterograde comets, potentially indicating epistasis between the manipulations (***Figure 4A, B***). However, we noted that the anterograde comets in the combined Shot knockdown/Mical overexpression neurons moved significantly faster than the retrograde comets, and also faster than the anterograde comets in the single manipulations (***Figure 4C***).

Movement of the anterograde comets in these neurons was also more irregular than in other samples, as these comets frequently slowed down and then sped up again (***Figure 4A***).

Conditions that cause mixed dendritic microtubule orientation also either cause c4da neuron dendrite pruning defects or enhance them (***Herzmann et al., 2018***). Mical overexpression alone does not cause pruning defects – in fact, it can suppress the pruning defects of certain ecdysone signaling mutants (***Kirilly et al., 2009***; ***Rode et al., 2018***). However, we observed a synergistic enhancement of the pruning defects caused by Shot knockdown when we overexpressed Mical (***Figure 4D–F***). Thus, our data suggest that Shot and actin cooperatively regulate dendritic microtubule orientation.

Shot is recruited to dendrite tips during early dendrite growth

As Shot is often recruited to specific subcellular locations via its actin binding domain (***Nashchekin et al., 2024***), we next assessed Shot localization in dendrites using GFP-tagged Shot constructs. We first visualized endogenously GFP-tagged Shot in third instar c4da neurons using structured illumination microscopy (SIM). In dendrite shafts, endogenously GFP-tagged Shot localized in closely spaced puncta close to the plasma membrane (***Figure 5A***), and transgenically expressed full-length Shot (Shot^{FL}::GFP) localized in a similar pattern (***Figure 5B***). We then visualized the two Shot variants lacking high affinity actin binding, Shot$^{\Delta CH1}$::GFP and Shot$^{\Delta ABD}$::GFP, and found that they also localized close to the plasma membrane in a very similar pattern to full-length Shot (***Figure 5C, D***). Thus, actin binding is unlikely to be required for Shot cortical localization in dendritic shafts.

The control of dendritic microtubule organization can likely be divided in early establishment and later maintenance processes. To assess potential Shot functions at other developmental stages, we investigated the localization of transgenic Shot::GFP from the first larval instar until the early pupal stage (***Figure 5—figure supplement 1***). Due to strong background from neighboring tissues, we were not able to visualize endogenously GFP-tagged Shot live and throughout the whole c4da neuron and used transgenic versions instead. Strikingly, we noted that Shot::GFP was highly enriched at dendrite tips in first instar c4da neurons, but could only be detected at low levels in the soma and proximal dendrites (***Figure 5E, H, I***). From the second instar onwards, Shot::GFP appeared relatively evenly distributed in the soma and along both axons and dendrites (***Figure 5—figure supplement 1***), indicating that Shot dynamically changes its localization during development.

To test whether Shot dendrite tip localization depends on actin, we next imaged the actin-binding-deficient variants Shot$^{\Delta CH1}$::GFP and Shot$^{\Delta ABD}$::GFP in first instar c4da neurons. Our estimates suggested that Shot$^{\Delta CH1}$::GFP was expressed at similar levels as wild-type Shot::GFP, while Shot$^{\Delta ABD}$::GFP was expressed at up to two times higher levels, making the localization patterns comparable. Shot$^{\Delta CH1}$::GFP accumulated in several dots per dendrite that could be many micrometers away from the tips (***Figure 5F, H***). Overall, significantly fewer distal dendrites were occupied by Shot$^{\Delta CH1}$::GFP compared to full-length Shot (***Figure 5F, I***). Shot$^{\Delta ABD}$::GFP was found at tips (***Figure 5G, I***), but always also localized in dots along dendritic shafts, such that there was no effective concentration at tips (***Figure 5G, H***). To independently test whether Shot tip localization is actin-dependent, we used UAS-Mical to disrupt actin. In c4da neurons overexpressing Mical, the Shot signal at tips was significantly broadened and Shot puncta could be seen along dendrite shafts (***Figure 5J, K***), similar to what was observed with Shot$^{\Delta ABD}$::GFP. We conclude that actin binding is required to transiently recruit and concentrate Shot at dendrite tips during the early stages of c4da neuron dendrite growth.

Shot acts early and is linked to end binding proteins

The observation that the Shot actin binding domain is required for both early dendrite tip localization and uniform dendritic microtubule orientation suggests that Shot function during early dendrite development is crucial for microtubule polarity. We therefore tested whether loss of Shot already causes defects in microtubule orientation during early development. When we imaged the directionality of EB1::GFP comets in primary dendrites of first instar c4da neuron dendrites, we indeed found a significant increase in plus end-out microtubules upon loss of Shot (***Figure 6A***).

To assess how Shot might affect microtubules at this stage, we next imaged mCherry-tagged α-tubulin live in first instar neurons and manipulated Shot levels. Interestingly, Shot overexpression caused a clear increase in mCherry::αtubulin in first instar dendrites (***Figure 6B, C***), suggestive of an increased microtubule density. Shot knockdown did not cause a significant decrease of the dendritic microtubule signal in this experiment (***Figure 6C***), but this could in part be due to technical reasons,

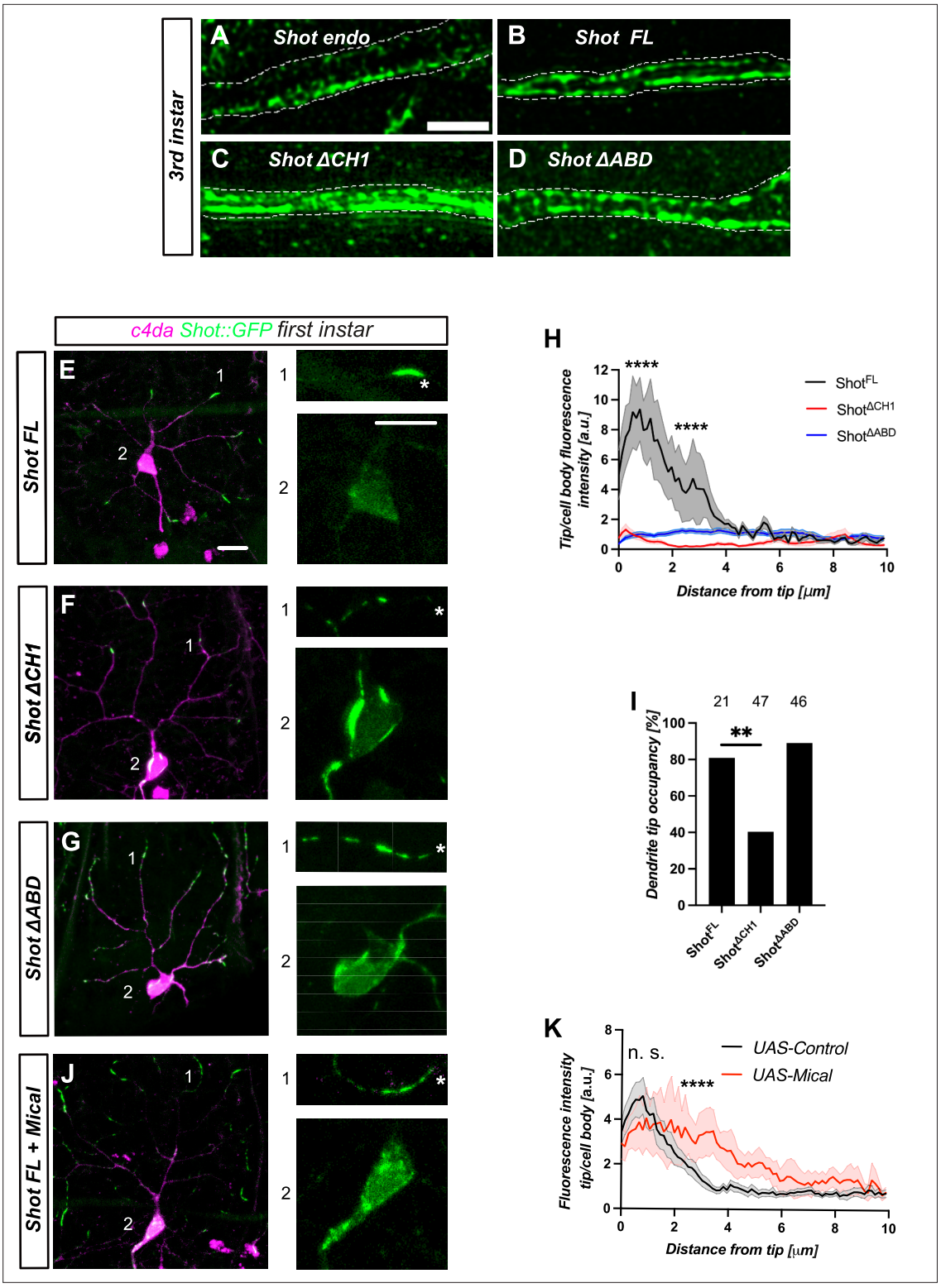


Figure 5. Shot is recruited to tips of growing dendrites via its actin binding domain. The indicated GFP-tagged Shot constructs and tdtomato were expressed in c4da neurons under *ppk-GAL4* and visualized at the indicated developmental stages. (**A–D**) Actin binding is not required for Shot localization in shafts of mature dendrites. The indicated Shot::GFP constructs were visualized in third instar primary c4da neuron dendrites by immunofluorescence followed by structured illumination microscopy. Borders of dendrites are indicated by white broken lines. (**A**) Endogenously tagged Shot::GFP. (**B**) Localization of transgenic full-length Shot (Shot^{FL}::GFP) expressed under *ppk-GAL4*. (**C**) Localization of Shot$^{\Delta CH1}$::GFP expressed under *ppk-GAL4*. (**D**) Localization of Shot$^{\Delta ABD}$::GFP expressed under *ppk-GAL4*. (**E–K**) Localization of the indicated Shot::GFP variants in first instar c4da

Figure 5 continued on next page

Figure 5 continued

neurons. Images on the right show close-ups of dendrite tip (1) and soma regions (2). Asterisks in the dendrite close-ups mark the position of the tip. (**E**) Localization of Shot^{FL}::GFP. (**F**) Localization of Shot$^{\Delta CH1}$::GFP. (**G**) Localization of Shot$^{\Delta ABD}$::GFP. (**H**) Fluorescence intensity profiles of Shot::GFP variants in the distal 10 µm of first instar dendrites in (**E**–**G**). Intensity values are normalized to Shot::GFP intensity in the cell body. Solid lines indicate average, envelopes indicate SD (*N* = 10 neurons). Compared to full-length Shot, GFP intensities of Shot$^{\Delta CH1}$ and Shot$^{\Delta ABD}$ in the 0–2 and 2–4 µm brackets from the tip were significantly reduced (****p < 0.0001, Mann–Whitney *U* test). (**I**) Dendrite tip occupancy of Shot::GFP variants in (**E**–**G**). **p < 0.01, Fisher's exact test. (**J**, **K**) Effect of Mical overexpression on Shot^{FL}::GFP localization. (**J**) Localization of Shot^{FL}::GFP in a c4da neuron overexpressing Mical. (**K**) Fluorescence intensity profiles of Shot^{FL}::GFP in the distal 10 µm of first instar dendrites with or without Mical overexpression. Shot::GFP intensity upon Mical overexpression was not significantly different from Shot::GFP without Mical in the 0–2 µm bracket, but highly significant in the 2–4 µm bracket (*N* = 10 neurons, p < 0.0001, Mann–Whitney *U* test). Scale bars are 5 µm in (**A**) and 10 µm in (**E**) (larger image and close-up).

The online version of this article includes the following figure supplement(s) for figure 5:

Figure supplement 1. Shot dendritic tip enrichment is transient.

as we could not use the strongest Shot manipulation (Shot knockdown only, instead of knockdown in a heterozygous *shot* mutant background). To visualize dendritic microtubule structure at high resolution with the stronger manipulation, we also used stimulated emission depletion (STED) microscopy imaging of third instar dendritic microtubules (***Figure 6—figure supplement 1***). While microtubules appeared as several continuous and bundled filaments in primary dendrites of control neurons, fewer filamentous structures were visible in dendrites of c4da neurons lacking Shot, the microtubule staining was more punctate, and the width of the microtubule bundles significantly thinner. Together with the domain analysis demonstrating the importance of the GAS2 domain, these data suggest that Shot promotes stabilization of dendritic microtubules.

Shot is known to bind to the plus end binding protein EB1 via several SxIP motifs in its C-terminal region (***Slep et al., 2005***; ***Alves-Silva et al., 2012***), and EB1 is also implicated in dendritic microtubule orientation (***Mattie et al., 2010***). In the presence of Shot::GFP, red fluorescently tagged EB1 also became recruited to dendrite tips at the first instar and colocalized with Shot::GFP (***Figure 6D, E***). This depended on the presence of the Shot C-terminal region including the SxIP motifs, as Shot$^{\Delta CTail}$ expression did not recruit EB1 (***Figure 6D, E***). Very rarely, EB1 comets could be seen emanating from a Shot/EB1-rich tip (***Figure 6—figure supplement 1***).

The minus end binder Patronin also interacts with Shot (***Nashchekin et al., 2016***) and is required for uniform plus end-in dendritic microtubule orientation in flies (***Wang et al., 2019***; ***Feng et al., 2019***) and worms (***He et al., 2022***). We confirmed in immunoprecipitation experiments that a Shot fragment comprising spectrin repeats 27–32 interacts with Patronin (***Figure 6—figure supplement 1***), similar to what has been reported for the mammalian Shot and Patronin homologues (***Noordstra et al., 2016***; ***Ning et al., 2016***). Similarly to Shot, the mechanism of Patronin in dendritic microtubule orientation likely involves microtubule stabilization (by protecting minus ends from depolymerization) (***Wang et al., 2019***). Patronin knockdown caused an increase in the frequency of plus end-out microtubules in primary dendrites already at the first instar stage (***Figure 6F***), and a heterozygous P element mutant in *Patronin* significantly increased the percentage of plus end-out microtubules at the third instar when combined with Shot knockdown (***Figure 6G***). We also tested for genetic interactions between Shot and end binding proteins using pruning as readout and found that both the heterozygous *Patronin* mutant and a dsRNA construct targeting EB1 strongly enhanced the pruning phenotypes seen upon shot knockdown (***Figure 6H–K***). Similarly to Shot, both knockdown of Patronin and EB1 also caused c4da neuron dendrite regrowth defects at 72 h APF (***Figure 1—figure supplement 1***). Thus, Shot likely cooperates closely with end binders to orient dendritic microtubules during early dendrite development.

Rab11 is linked to dendritic microtubule regulation in c4da neurons

A tip-based mechanism for microtubule orientation has first been proposed in *C. elegans* PVD sensory neurons, where Rab11-positive vesicles are part of a transient ncMTOC that localizes to the tips of growing dendrites (***Liang et al., 2020***; ***Harterink et al., 2018***). We therefore asked whether a similar transient MTOC would also exist in *Drosophila* sensory neurons. In *Drosophila* sensory neurons, vesicle-based dendritic MTOCs have been proposed on either Golgi outposts (***Ori-McKenney et al., 2012***; ***Mukherjee et al., 2020***; ***Yalgin et al., 2015***) or Rab5 endosomes (***Nguyen et al., 2014***; ***Weiner***

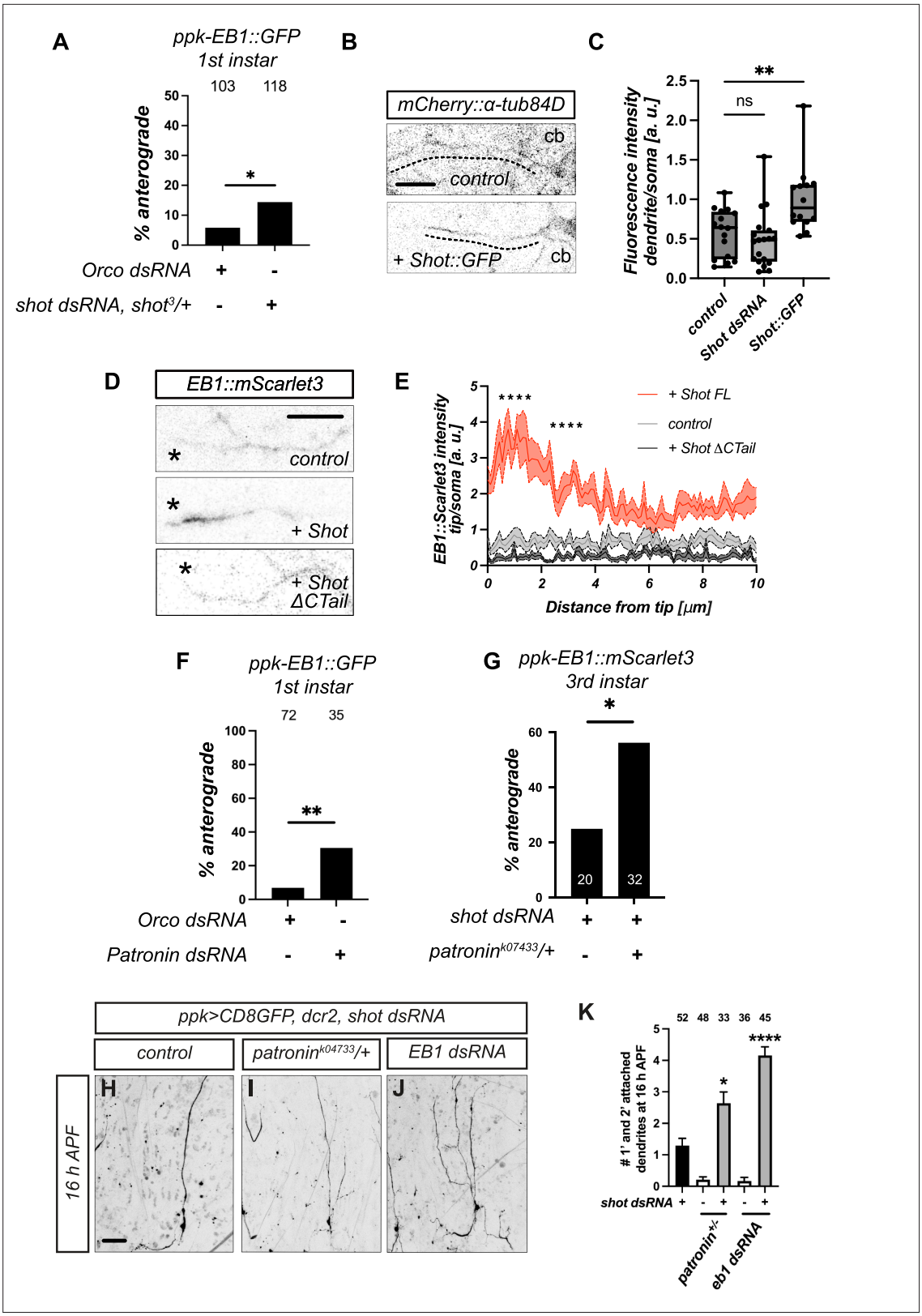


Figure 6. Shot acts during early development and interacts with end binding proteins. (**A**) Frequency of anterograde EB1 comets at the first instar stage in control (Orco dsRNA) and shot knockdown neurons (shot dsRNA, *shot*^{3}/+). Number of comets per sample is shown in the graph (14 and 20 neurons, respectively, range 0–40% anterograde per neuron), *p < 0.05, Mann–Whitney *U* test. (**B**) Microtubules in dendrites of first instar control neurons or neurons expressing Shot::GFP were visualized using mCherry-tagged α-tubulin in single confocal slices. (**C**) Dendritic microtubule density for samples

Figure 6 continued on next page

Figure 6 continued

in (**B**). Dendritic mCherry-α-tubulin 84B fluorescence intensity was normalized to that of the soma. *N* = 14–22 dendrites from 9 to 14 neurons, *p < 0.05, Student's *t*-test. (**D**) Shot can recruit EB1 to dendrite tips. EB1::mScarlet3 was expressed in c4da neurons alone, with Shot^{FL}::GFP, or with Shot$^{\Delta CTail}$::GFP, and visualized at the first instar larval stage. Positions of dendrite tips are indicated by asterisks. (**E**) Fluorescence intensity profiles of EB1::mScarlet3 in the distal 10 µm of first instar dendrites. Solid lines indicate average, envelopes indicate SEM (*N* = 9–10 dendrites, 3 neurons each). Significance between genotypes was calculated for 0–2 and 2–4 µm distances from the tip. ****p < 0.0001, Mann–Whitney *U* test. (**F**) Frequency of anterograde EB1 comets at the first instar stage in control (Orco dsRNA) and *patronin* knockdown neurons (patronin dsRNA). Number of comets is shown in the graph (8 and 9 neurons, respectively, range 0–66% anterograde for each neuron). **p < 0.01, Mann–Whitney *U* test. (**G**) Frequency of anterograde EB1 comets at the third instar stage in *shot* knockdown neurons (*shot* dsRNA) and *shot* knockdown neurons in a heterozygous *patronin* mutant background. Number of comets is shown in the graph (8 and 11 neurons, respectively, range 0–80% anterograde for each neuron). *p < 0.05, Mann–Whitney *U* test. (**H–K**) Synergistic genetic interactions between *shot* and end binding proteins during c4da neuron dendrite pruning. (**H–J**) *shot* dsRNA was expressed in c4da neurons of animals in the indicated backgrounds, and pruning defects were quantified at 16 h APF. (**H**) C4da neuron expressing *shot* dsRNA. (**I**) C4da neuron expressing *shot* dsRNA in a *patronin*/+background. (**J**) C4da neuron co-expressing *shot* and *EB1* dsRNAs. (**I**) Severity of pruning defects in (**H–J**) and in respective controls. *N* = 33–52 neurons, **p < 0.01, ****p < 0.0001, Wilcoxon's test. Scale bars are 5 µm in (**B**), 2 µm in (**D**), and 50 µm in (**E**).

The online version of this article includes the following source data and figure supplement(s) for figure 6:

Figure supplement 1. Shot affects microtubule appearance and interacts with tip binding proteins.

Figure supplement 1—source data 1. Original files for Western analysis displayed in ***Figure 6—Figure Supplement 1D***.

Figure supplement 1—source data 2. Pdf file with original files Western analysis displayed in ***Figure 6—Figure Supplement 1D*** with labeled bands.

et al., 2020), and microtubules have been observed originating in dendritic shafts, at branchpoints and at tips (***Mukherjee et al., 2020***; ***Yalgin et al., 2015***; ***Weiner et al., 2020***; ***Liang et al., 2020***).

We and others have shown that Rab11 is required for c4da neuron dendrite pruning via an unclear mechanism (***Krämer et al., 2019***; ***Lin et al., 2020***). To test whether *Drosophila* Rab11 interacts with microtubule regulators involved in pruning regulation, we used immunoprecipitation of tagged proteins from transfected S2 cells. This showed that Rab11 could be co-precipitated with the microtubule polymerase and MTOC component Msps/XMAP215, which has been linked to pruning and dendritic microtubule organization (***Tang et al., 2020***; ***Figure 7A***). This interaction depended on GTP binding by Rab11, as GTP-binding-deficient Rab11 S25N showed a reduced interaction with Msps (***Figure 7A***). We next asked whether Rab11 colocalizes with potential MTOC components in c4da neuron dendrites using fluorescently tagged transgenes. At the first instar, Rab11::mCherry puncta could be seen overlapping with γ-tubulin::GFP both at dendrite branchpoints and tips (***Figure 7B***). To test whether such puncta could nucleate microtubules, we observed Rab11::mCherry together with EB1::GFP. In first instar neurons, a fraction of EB1::GFP comets could be observed originating at dendritic Rab11::mCherry puncta (6/9 neurons, 10/58 comets) in dendritic shafts or at branchpoints (***Figure 7C, D***). All of these comets moved retrogradely (10/10). Partially because of low EB1::GFP fluorescence, we could not detect dendrite tips – or comets originating from tips – in these experiments. In support of the idea that this Rab11/microtubule link might be transient, no EB1::GFP comets emanating from Rab11::mCherry puncta could be observed at the third instar stage (0/9 neurons, 27 comets) (***Figure 7D***). Due to strong expression of γ-tubulin::GFP, we could not determine whether Rab11 still colocalizes with γ-tubulin at this stage. We next knocked down Rab11 and Rab5 and assessed the effects on microtubule orientation. Knockdown of Rab11, but not Rab5, caused a significant increase in the fraction of anterograde EB1 comets (***Figure 7E, F***) as well as increased comet speed at the third instar stage (***Figure 7G***). At the first instar stage, Rab11 knockdown caused a milder increase in anterograde comets that was not significant (***Figure 7—figure supplement 1A***). Thus, our evidence links Rab11 to dendritic microtubule regulation in *Drosophila* c4da neurons, but in part for technical reasons we cannot be certain whether it acts through the same tip-based mechanism as in *C. elegans* PVD.

As Shot has previously been shown to regulate Rab11 localization in epithelia (***Khanal et al., 2016***), we tested whether the two factors might also act in a common pathway in dendrites. We first used pruning phenotypic strength to assess a potential genetic interaction and found that Rab11 knockdown in a *shot*^{3}/+heterozygous background caused significantly more higher order dendrites to stay attached to the soma than with Rab11 knockdown alone, indicative of enhancement (***Figure 7H–J***). To observe potential effects in dendrites more directly, we expressed GFP-tagged Rab11 and visualized it using live microscopy at the first instar stage. Rab11::GFP vesicles in dendrites could be found along the whole dendritic shaft and were highly mobile (***Figure 7K***). However, neither the mobility nor the

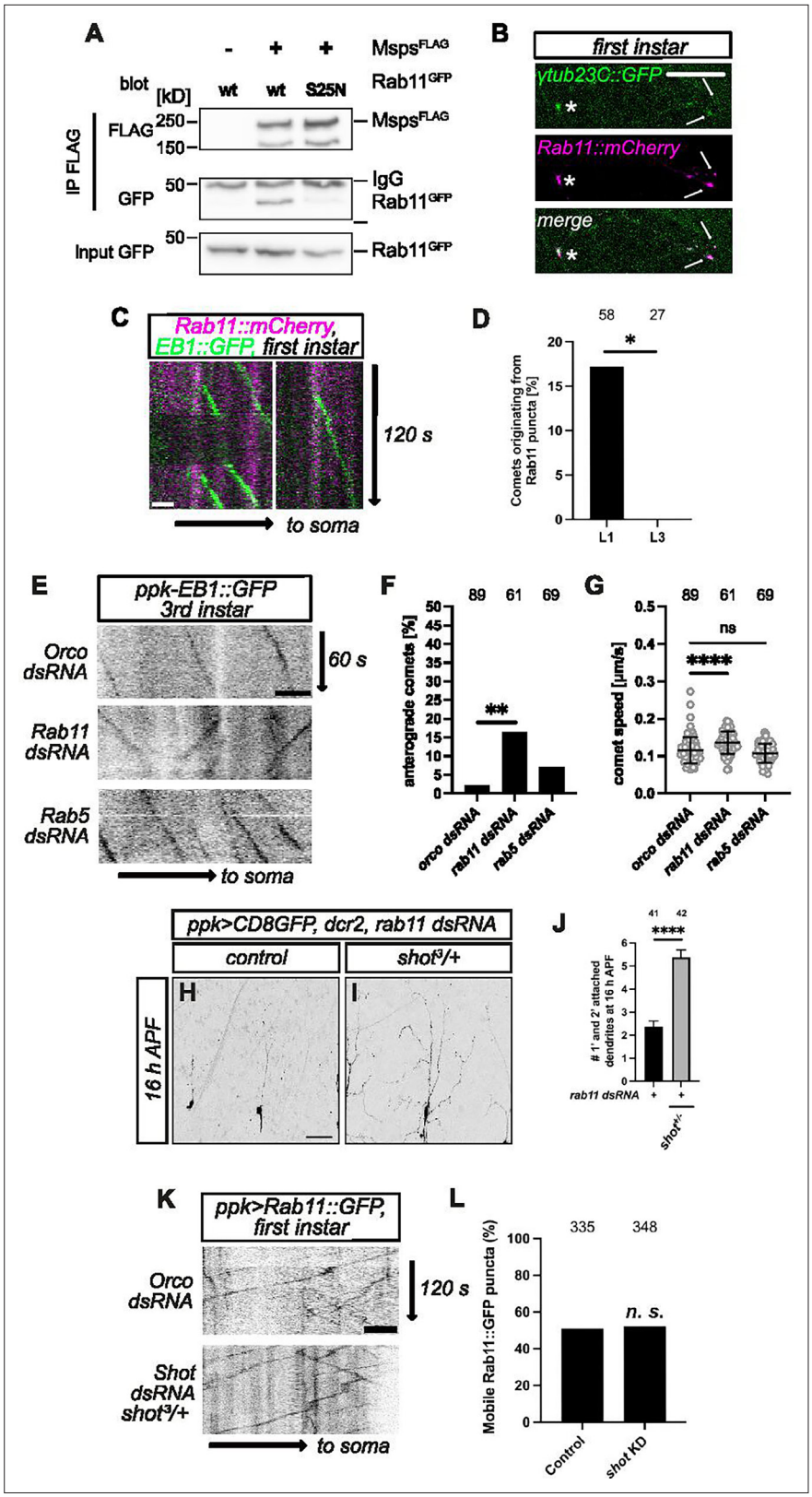


Figure 7. Evidence that Rab11 is linked to developmental dendritic microtubule regulation. (**A**) GFP-tagged Rab11 (wt or S25N) and FLAG-tagged Msps were cotransfected into S2 cells and immunoprecipitated with FLAG beads. Inputs and immunoprecipitates (IP) were blotted with the indicated antibodies. Sizes of molecular weight markers in kiloDalton (kD) are shown. IgG denotes antibody heavy chains. (**B**) Rab11 colocalizes with the

Figure 7 continued on next page

Figure 7 continued

microtubule organizing center (MTOC) marker γ-tubulin in growing c4da neuron dendrites. Rab11::mCherry and γ-tubulin23C::GFP were coexpressed under *ppk-GAL4* and visualized at the first instar. Arrows show Rab11/γ-tubulin-positive puncta at dendrite tips; the asterisk denotes a double-positive dot at a branchpoint. (**C**) Microtubules can originate at Rab11 puncta in dendrites. Rab11::mCherry and EB1::GFP were coexpressed in c4da neurons, and EB1 comets were visualized at the first instar. Example kymographs show Rab11::mCherry (magenta) and EB1::GFP (green). (**D**) Percentage of EB1 comets arising from dendritic Rab11 puncta at the first and third instars. Number of comets is shown in the graph. *p < 0.05, Fisher's exact test. (**E**) Effect of Rab11 knockdown on dendritic microtubule orientation. Kymographs show EB1::GFP movement in third instar c4da neuron dendrites. Upper panel: control c4da neuron expressing Orco dsRNA; middle panel: c4da neuron expressing Rab11 dsRNA; lower panel: c4da neuron expressing Rab5 dsRNA. (**F**) Penetrance of anterograde comets in (**E**). Number of comets is shown in the graph. **p < 0.01, two-tailed Fisher's exact test. (**G**) Speed of EB1::GFP comets in (**E**). ****p < 0.0001, Wilcoxon's test. (**H–J**) Rab11 and Shot interact genetically during dendrite pruning. *Rab11* dsRNA was expressed in c4da neurons of control animals (**H**) or in a $shot^3$/+heterozygous background (**I**), and neurons were visualized at 16 h APF. (**J**) Severity of pruning defects in (**H**) and (**I**). *N* = 41 and 42 neurons. ****p < 0.0001, Wilcoxon's test. (**K**) Kymograph analysis of Rab11::GFP movement in dendrites of first instar control c4da neurons or *shot* knockdown neurons (lower panel). (**L**) Fraction of mobile Rab11::GFP particles in samples in (**K**). Number of Rab11::GFP particles is shown in the graph. n.s., not significant, Fisher's exact test. Scale bars are 5 μm in (**B**), (**C**), (**E**), and (**K**), and 50 μm in (**H**).

The online version of this article includes the following source data and figure supplement(s) for figure 7:

Source data 1. Original files for Western analysis displayed in ***Figure 7A***.

Source data 2. Pdf file with original files Western analysis displayed in ***Figure 7A*** with labeled bands.

Figure supplement 1. Effect of Rab11 knockdown on microtubule polarity at the first instar, model.

overall localization of these puncta were changed upon shot knockdown (***Figure 7L***). Thus, Shot is unlikely to directly regulate Rab11 trafficking in dendrites.

Discussion

Microtubule orientation in neurites is crucial for neuronal polarity and developmental processes like neurite pruning, but the mechanisms that shape neuronal microtubule organization during development are still emerging. Here, we show that the spectraplakin Shot is required for the uniform plus end-in organization of dendritic microtubules. Our data suggest that Shot acts in a developmental timing-dependent fashion by selectively stabilizing microtubules at dendrite tips. This model is based on the following observations: firstly, Shot transiently localizes to dendrite tips in early growing dendrites, and the domains required for localization are required for microtubule orientation. Several lines of evidence show that this localization is actin-dependent. Shot mutants lacking the ability to bind actin with high affinity showed altered localization at dendrite tips at the first instar, and enzymatic disruption of F-actin by Mical overexpression also altered Shot localization. Shot recruitment may therefore be mediated via a transient actin-rich growth cone-like structure. The fact that we did not observe strong actin enrichment at dendrite tips (or a strong decrease in neurons overexpressing Mical) may be due to limitations of lifeact::GFP as the actin probe. For one, lifeact::GFP also fluoresces when not bound to actin. In addition, it has recently been shown in *Drosophila* oocytes that Shot binds to actin structures that are only weakly labeled by lifeact::GFP (***Nashchekin et al., 2024***). Importantly, the actin-binding domain required for tip recruitment is also required for correct microtubule orientation, indicating that Shot acts via a tip-based mechanism to orient microtubules. Secondly, the main function of Shot is likely to be microtubule stabilization via the GAS2 domain, which is required for Shot's function in microtubule orientation (***Figure 3***). The surprising finding that this region of Shot is sufficient to rescue Shot function in the absence of the large spectrin repeat region also supports this model and is consistent with the idea that Shot is regulated via autoinhibition, and actin binding may be required to disinhibit it (***Applewhite et al., 2013***). In addition to direct microtubule stabilization via the GAS2 domain, Shot can recruit the plus end binder EB1 (and potentially Patronin) (***Figure 6***) to increase microtubule stability. We think that such a local mechanism could also be sufficient for the observed increase in microtubule signal along the whole dendrite upon Shot overexpression at the first instar stage, especially since then dendrites are still relatively short.

This tip-based mechanism is reminiscent of the mechanism in the *C. elegans* PVD neuron, where a transient MTOC exists at tips of early growing dendrites. It was recently shown that in addition to bundling and stabilization, GAS2 domains can also nucleate microtubules in vitro (***An et al., 2025***). We think that it is unlikely that Shot itself acts to nucleate microtubules at dendrite tips because we were not able to detect an increase in microtubule nucleation from tips upon Shot overexpression. However, it is interesting to speculate that selective local microtubule stabilization at tips may already be sufficient to favor plus end-in polarity if the microtubules generated in other regions are sufficiently unstable, and microtubules from tips can only grow in the retrograde direction (***Figure 7—figure supplement 1B***). This idea could be tested through mathematical modeling. However, it is also possible that other, additional MTOC components localize to early dendrite tips in *Drosophila* sensory neurons as well. One candidate here is Rab11, which our analysis links to dendritic microtubule regulation, even though we did not see Rab11 enriched at tips. It is possible that the first instar stage, when most of our reagents start to work reliably, is already too late to visualize some of the very early growth events. Alternatively, the minus end-binder Patronin has been proposed to promote microtubule growth at minus ends (***Feng et al., 2019***). As Patronin is already required for microtubule orientation at the first instar, it is also interesting to speculate that Shot might capture and stabilize microtubules that grow in this way. In our model, Shot acts to set up plus end-in microtubule orientation early during development, and this orientation can then be maintained by mechanisms such as guidance along existing microtubules (***Mattie et al., 2010***). Our data suggest that early-stage tip-based microtubule regulation is a general feature of dendritic development.

Our data also do not rule out that Shot could anchor and stabilize dendritic microtubules in mature third instar neurons, likely in cooperation with actin. Loss of Shot in combination with actin disassembly caused unusual comet behaviors (***Figure 4***), possibly indicative of sliding, for example, through defective microtubule anchoring (***He et al., 2020***). Local membrane-bound microtubule stabilizers have been linked to the maintenance of dendritic microtubule orientation (***He et al., 2020***; ***Liang et al., 2025***), and Shot might have a similar function. Alternatively, the observation that only the plus end-out oriented subset of comets is fast-moving could point to a different origin of these microtubules, for example, they could enter the dendrites from the soma. Interestingly, local membrane-anchoring of microtubules also plays a role in axonal microtubule orientation, where recruitment of end-binding proteins to the axon initial segment by the adaptor protein AnkG is important for plus end-out orientation.

Last but not least, our data again confirm our notion that uniform plus end-in dendritic microtubule orientation is required for c4da neuron dendrite pruning, as all Shot manipulations leading to a more mixed orientation caused pruning defects. As we do not have evidence for Shot regulation at the onset of the pupal stage (e.g., ***Figure 5—figure supplement 1***), the function of Shot crucial for pruning is most arguably its early role in setting up uniform microtubule orientation.

Materials and methods

Key resources table

Reagent type (species) or resource	Designation	Source or reference	Identifiers	Additional information
Genetic reagent (*D. melanogaster*)	ppk-Gal4, UAS-CD8GFP	***Grueber et al., 2007***		
Genetic reagent (*D. melanogaster*)	ppk-Gal4, UAS-tdtomato	***Herzmann et al., 2017***		
Genetic reagent (*D. melanogaster*)	R57C10-GAL4	Bloomington Drosophila Stock Center	BDSC:605712; FLYB:FBst000605712; RRID:BDSC_605712	
Genetic reagent (*D. melanogaster*)	w;FRT G13 shot(3)/CyO	Bloomington Drosophila Stock Center	BDSC:5141; FLYB:FBst0005141; RRID:BDSC_5141	

Continued on next page

Continued

Reagent type (species) or resource	Designation	Source or reference	Identifiers	Additional information
Genetic reagent (*D. melanogaster*)	SOP-FLP	***Matsubara et al., 2011***		
Genetic reagent (*D. melanogaster*)	y(1) v(1); P{y[+t7.7] v[+t1.8]=TRiP. JF02971}attP2	Bloomington Drosophila Stock Center	BDSC:28336; FLYB:FBst00028336; RRID:BDSC_28336	Shot RNAi line
Genetic reagent (*D. melanogaster*)	y(1) v(1); P{y[+t7.7] v[+t1.8]=TRiP. JF01219}attP2	Bloomington Drosophila Stock Center	BDSC:31278; FLYB:FBst00031278; RRID:BDSC_31278	Used as control RNAi line
Genetic reagent (*D. melanogaster*)	w[1118]; P{GD11761}v22198	Vienna Drosophila Resource Center	VDRC v22198 RRID:VDRC_22198	UAS Rab11 RNAi
Genetic reagent (*D. melanogaster*)	w[1118]; P{GD10492}v34096	Vienna Drosophila Resource Center	VDRC v34096 RRID:VDRC_34096	UAS-Rab5 RNAi
Genetic reagent (*D. melanogaster*)	w[1118]; P{GD13490}v24451	Vienna Drosophila Resource Center	VDRC v24451 RRID:VDRC_24451	UAS-EB1 RNAi
Genetic reagent (*D. melanogaster*)	w[*]; P{w[+mC]=UAS-shot.L(C)-GFP}3	Bloomington Drosophila Stock Center	BDSC:29043; FLYB:FBst00029043; RRID:BDSC_29043	UAS-ShotΔCH1::GFP
Genetic reagent (*D. melanogaster*)	w[*] P{w[+mC]=UAS-shot.L(A)-GFP}1	Bloomington Drosophila Stock Center	BDSC:29044; FLYB:FBst00029044; RRID:BDSC_29044	UAS-Shot::GFP (X)
Genetic reagent (*D. melanogaster*)	w[*]; P{w[+mC]=UAS-shot.L(A)-GFP}1	this study		UAS-Shot::GFP, hopped to third chromosome
Genetic reagent (*D. melanogaster*)	w[1118]; PBac{y[+mDint2] w[+mC]=UAS-shot.RE-DeltaABD.GFP} VK00031	Bloomington Drosophila Stock Center, ***Hahn et al., 2021***	BDSC:93282; FLYB:FBst00093282; RRID:BDSC_93282	UAS-ShotΔABD::GFP
Genetic reagent (*D. melanogaster*)	w; P{w[+mC]=UAS-shot.L(A)ΔCTail-GFP}	Gift from A. Prokop		UAS-ShotΔCTail::GFP
Genetic reagent (*D. melanogaster*)	Shot PBac{ shot::YFP}	***Nashchekin et al., 2016***		Genomic Shot wt rescue on third chr.
Genetic reagent (*D. melanogaster*)	P{UASp-shot.C.YFP}	***Nashchekin et al., 2024***		Shot CTerm::YFP
Genetic reagent (*D. melanogaster*)	SHot::GFP(endo)	***Voelzmann et al., 2026***		Endogenously GFP-tagged Shot
Genetic reagent (*D. melanogaster*)	UAS-kin::lacZ	***Clark et al., 1997***		
Genetic reagent (*D. melanogaster*)	UAS-Mical	***Terman et al., 2002***		

Continued on next page

Continued

Reagent type (species) or resource	Designation	Source or reference	Identifiers	Additional information
Genetic reagent (*D. melanogaster*)	y(1) w[*]; P{y[+t*] w[+mC]=UAS-Lifeact-GFP}VIE-260B	Bloomington Drosophila Stock Center	BDSC:35544; FLYB:FBst00035544; RRID:BDSC_35544	
Genetic reagent (*D. melanogaster*)	UAS-αtub84B::mCherry	***Villars et al., 2022***		
Genetic reagent (*D. melanogaster*)	w[*]; P{w[+mC]=UAS-Rab11-GFP}2	Bloomington Drosophila Stock Center	BDSC:8506; FLYB:FBst0008506; RRID:BDSC_8506	
Genetic reagent (*D. melanogaster*)	UAS-γtub23C::GFP	***Nguyen et al., 2011***		
Genetic reagent (*D. melanogaster*)	UAS-cytoABKAR TA	***Marzano et al., 2021***		
Genetic reagent (*D. melanogaster*)	UAS-Brp^{short}::Strawberry	Other		Gift from S. Sigrist, FU Berlin
Genetic reagent (*D. melanogaster*)	UAS-EB1::GFP	***Zheng et al., 2008***		
Genetic reagent (*D. melanogaster*)	ppk-EB1::GFP	***Arthur et al., 2015***		
Genetic reagent (*D. melanogaster*)	UAS-EB1::mScarlet3	This study		See Materials and methods section
Genetic reagent (*D. melanogaster*)	UAS-Rab11::mCherry	This study		See Materials and methods section
Genetic reagent (*D. melanogaster*)	ppk-EB1::mScarlet3	This study		See Materials and methods section
Genetic reagent (*D. melanogaster*)	w[1118]; P{w[+mC]=UAS-Dcr-2.D}2	Bloomington Drosophila Stock Center	BDSC:24650; FLYB:FBst00024650; RRID:BDSC_24650	
Genetic reagent (*D. melanogaster*)	y(1) w[*]; P{y[+t7.7] w[+mC]=UAS-Cas9.P2}attP40	Bloomington Drosophila Stock Center	BDSC:58985; FLYB:FBst00058985; RRID:BDSC_58985	
Genetic reagent (*D. melanogaster*)	U6:1 U6:3-Shot tandem sgRNA	This study		
Genetic reagent (*D. melanogaster*)	P{ry[+t7.2]=neoFRT}42D P{w[+mC]=lacW}l(2)k07433[k07433] / CyO y[+]	Kyoto Stock Center	Stock # 111217 RRID:DGGR_111217	
Cell line (*D. melanogaster*)	S2R+	DGRC	FBtc0000150; RRID:CVCL_Z831	
Antibody	anti-beta-galactosidase (Rabbit polyclonal)	Cappel	Cat# 55976, RRID:AB_2313707	IF (1:700)
Antibody	anti-GFP (Chicken polyclonal)	Aves labs	Cat# GFP-1020 RRID:AB_2307313	IF (1:500)

Continued on next page

Continued

Reagent type (species) or resource	Designation	Source or reference	Identifiers	Additional information
Antibody	anti-GFP (Rabbit polyclonal)	Thermo Fisher	Cat# A11122 AB_221569	IF (1:1000)
Antibody	anti-GFP 3E6 (Mouse monoclonal)	Thermo Fisher	Cat# A11120 RRID:AB_221568	IF (1:500)
Antibody	anti-mCherry 16D7 (Rat monoclonal)	Thermo Fisher	RRID:AB_2536611	IF (1:1000)
Antibody	anti-DsRed (Rabbit Polyclonal)	Clontech	Cat# 632496 RRID:AB_10013483	WB (1:1000)
Antibody	anti-22C10 (Mouse monoclonal)	DSHB	AB_528403 RRID:AB_528403	IF (1:50)
Antibody	anti-GFP JL-8 (Mouse monoclonal)	Clontech	Cat# 632380 RRID:AB_10013427	WB (1:1000)
Antibody	anti-FLAG M2 (Mouse monoclonal)	Sigma	Cat# F3165 RRID:AB_259529	WB (1:5000)
Antibody	anti-myc 9E10 (Mouse monoclonal)	DSHB	RRID:AB_2266850	WB (1:50)
Antibody	anti-mouse 488 (Goat polyclonal)	Invitrogen	A10680 RRID:AB_2534062	IF (1:1000)
Antibody	anti-mouse 568 (Goat polyclonal)	Invitrogen	A11031 RRID:AB_144696	IF (1:1000)
Antibody	anti-rabbit 488 (Goat polyclonal)	Invitrogen	A11008 RRID:AB_143165	IF (1:1000)
Antibody	anti-rabbit 568 (Goat polyclonal)	Invitrogen	A11011 RRID:AB_143157	IF (1:1000)
Antibody	STAR-RED-conjugated goat anti-Rat IgG	abberior	Cat# STRED-1007 RRID:AB_2910106	IF (1:200)
Antibody	goat-anti-Rabbit IgG, HRP-conjugated	Dianova	DNA-SEC-183364	WB (1:7500)
Antibody	goat-anti-Mouse IgG, HRP-conjugated	Dianova	DNA-SEC-183170	WB (1:7500)
Recombinant DNA reagent	pUAST attB-Rab11::GFP (plasmid)	This study		See Materials and methods section
Recombinant DNA reagent	pUAST attB-Rab11::GFP S25N (plasmid)	This study		See Materials and methods section
Recombinant DNA reagent	pUAST attB-Msps::FLAG (plasmid)	This study		See Materials and methods section
Recombinant DNA reagent	pUAST attB-GFP::Patronin (plasmid)	This study		See Materials and methods section
Recombinant DNA reagent	pUAST attB-myc::Shot 3626–4248 (plasmid)	This study		See Materials and methods section
Recombinant DNA reagent	pCFD4 w+attB-Shot sgRNA (plasmid)	This study		See Materials and methods section
Sequence-based reagent	Shot sgRNA#1	This study	sgRNA	GCTGCCCTCTCAGGCCGATT
Sequence-based reagent	Shot sgRNA#2	This study	sgRNA	GAGTTCTCCAGAGTGGTCAC
Sequence-based reagent	linker primer for EB1::mScarlet3	This study		CACACCTCCACTACCGCTAGCAGGCCGG CCACGCGTGGTACCTTCTGGTCCA
Commercial assay or kit	pENTR/D-TOPO Cloning Kit	Thermo Fisher	K240020	

Continued on next page

Continued

Reagent type (species) or resource	Designation	Source or reference	Identifiers	Additional information
Chemical compound, drug	cOmplete protease inhibitor, EDTA-free	Roche	04693132001	
Software, algorithm	Fiji	Fiji	RRID:SCR_002285	
Software, algorithm	Prism	GraphPad	RRID:SCR_002798	
Other	Protein A sepharose	GE Healthcare	17-5280-01	
Other	anti-FLAG beads	Sigma	A-2220 RRID:AB_10063035	
Other	FuGENE transfection reagent	Promega	E5911	
Other	Halocarbon oil 700	Sigma	H8898	

Fly strains

C4da neurons were labeled by UAS-CD8::GFP or UAS-tdtomato expression under *ppk-GAL4* (**Grueber et al., 2007**). MARCM clones of *shot*^{3} mutants (BL 5141) were induced with *SOP-FLP* (**Matsubara et al., 2011**) and labeled by tdtomato expression under *nsyb-GAL4*^{R57C10}. Endogenously tagged Shot::GFP was from **Voelzmann et al., 2026** and the BAC carrying the SHOT genomic locus with a YFP tag was from **Nashchekin et al., 2016**. UAS transgenes were UAS-Shot^{RE}::GFP on the X chromosome (BL 29044), or mobilized to the third chromosome (this study), UAS-Shot^{RC}::GFP (ΔCH1, BL 29042), UAS-Shot$^{\Delta ABD}$::GFP (**Hahn et al., 2021**), UAS-Shot$^{\Delta CTail}$::GFP (**Alves-Silva et al., 2012**), UASp-Shot Cterm::YFP (**Nashchekin et al., 2016**), UAS-kin::lacZ (**Clark et al., 1997**), UAS-Mical (**Terman et al., 2002**), UAS-αtub84B::mCherry (**Villars et al., 2022**), UAS-Rab11::GFP (BL 8506), UAS-γtub23C::GFP (**Nguyen et al., 2011**), and UAS-cytoABKAR TA (**Marzano et al., 2021**) as inert UAS control, UAS-Brp^{short}::Strawberry to label presynapses (gift from S. Sigrist). EB1 analyses were carried out using either UAS-EB1::GFP (**Zheng et al., 2008**), *ppk-EB1::GFP* (**Arthur et al., 2015**), UAS-EB1::mScarlet3 (gift from M. Rolls) or *ppk-EB1::mScarlet3* (this study). The following dsRNA lines were used: Orco (BL 31278) as control, Shot (BL 28336), Rab11 (VDRC 22198), Rab5 (VDRC 34096), EB1 (VDRC 24451). All dsRNAs were coexpressed with UAS-dcr2 (**Dietzl et al., 2007**), and the Shot sgRNA was coexpressed with UAS-Cas9P2 (BL58985). Additional mutant alleles were *patronin*^{k07433} (Kyoto 111217).

Cloning and transgenes

Shot sgRNAs GCTGCCCTCTCAGGCCGATT (target 1) and GAGTTCTCCAGAGTGGTCAC (target 2) were cloned into pCFD4w+ (gift from S. Schirmeier). For transgenesis, plasmids were injected into flies carrying the 86Fb acceptor site. For biochemical experiments, the Rab11 ORF was cloned into pUAST attB carrying a C-terminal GFP tag using TOPO/TA cloning. The S25N mutation was inserted by PCR mutagenesis. N-terminally GFP-tagged Patronin was cloned into pUAST using standard restriction sites. To express the Shot spectrin repeats 27–32, a fragment of the Shot ORF encoding amino acids 3626–4248 was cloned into pUAST carrying a N-terminal myc tag via TOPO/TA cloning. For Rab11::mCherry flies, the Rab11 entry clone was used to generate pUAST attB Rab11::mCherry, the insert was subcloned into pUAST, which was then injected into *w*^{1118} flies using classical transposase-mediated transgenesis. To generate EB1::mScarlet3, a *Drosophila* codon optimized mScarlet3 (**Gadella et al., 2023**, synthesized by Twist Bioscience) was added after the EB1 coding sequence separated by a CACACCTCCACTACCGCTAGCAGGCCGGCCACGCGT GGTACCTTCTGGTCCA linker and cloned into pUAST. The resulting plasmid was injected into wild type embryos by Bestgene. The same insert was also inserted into the pDEST-APHIH vector carrying a *ppk* promoter fragment and injected into attP2 flies to generate *ppk-EB1::mScarlet3* flies. C-terminally FLAG-tagged Msps (isoform RB) was cloned into pUAST attB using standard cloning procedures.

Immunofluorescence

Briefly, appropriately staged pupal filets were fixed in 4% formaldehyde, blocked in PBS with 0.3% Triton X-100 and 10% goat serum, and incubated with antibody in blocking buffer overnight. C4da neurons labeled by *ppk* promoter fusions, endogenous or transgenic GFP-tagged Shot were visualized with chicken (1:500, Aves labs), rabbit (1:1000, Invitrogen A11122) or mouse (1:1000, Invitrogen A1120) anti-GFP. Tdtomato and mCherry-tagged transgenes were detected with rat anti-mCherry (1:1000, Invitrogen) or rabbit anti-DsRed antibodies (1:1000, Clontech). Kin::β-galactosidase fusion proteins were detected with rabbit anti-β-galactosidase (Cappel, preabsorbed in-house, 1:700), and *Drosophila* futsch was detected with 22C10 (DSHB, 1:50). Secondary antibodies for regular immunofluorescence were conjugated to Alexa Fluor 488, 568, or 647. For STED microscopy of tagged tubulin, Abberior anti-rabbit STAR RED were used as secondary antibodies.

Microscopy, time lapse imaging

For analyses of dendrite pruning phenotypes at 16 h APF, animals were dissected out of the pupal case and mounted in 90% glycerol/PBS. Dorsal ddaC c4da neurons in segments A2–A5 were imaged live on a Zeiss LSM710 confocal microscope with a 20x Plan Apochromat water objective (1.0 NA). For regrowth analyses at 72 h APF, animals were dissected out of the pupal case and ventral v'ada c4da neurons in segments A2–A4 were imaged as described (***Sanal et al., 2023***). For live protein localization analyses, first instar larvae were immobilized on double-sided tape and mounted in Halocarbon oil 700; third instar larvae were briefly anesthetized with ether before imaging. Neurons were then imaged live on a Zeiss LSM880 microscope with a 63x Plan Apochromat DIC M27 oil objective (1.4 NA). For EB1::GFP or EB1::mScarlet3 live imaging, third instar larvae were anesthetized with ether, and first instar larvae were immobilized on double-sided tape. Live analysis was performed on a Zeiss LSM880 microscope using a 40x Plan Apochromat FCS M27 (1.2 NA) oil objective. Consecutive images of a single plane were taken every second for 1–2 min; Z positions were adjusted if larvae moved. Movies were stabilized with the Fiji Image Stabilizer plugin, and the KymoResliceWide plugin was used to generate EB1 comet kymographs. Comet speed was read out manually from kymographs.

Immunofluorescence images of kin::lacZ were obtained on a Zeiss LSM 710 microscope using a 40x Zeiss C Apochromat water objective (1.1 NA). SIM was performed on a Zeiss Elyra 7 microscope with a 63x Plan Apochromat DIC M27 oil objective (1.4 NA) with an Edge 4.2 SIM camera (50-ms exposure time), and deconvolution was done using SIM^2 software. All microscopes used ZEN Black software. Most STED microscopy images were taken with an abberior FACILITY LINE (Abberior Instruments GmbH) equipped with an inverted IX83 microscope (Olympus), a 60x oil objective (Olympus UPLXAPO 60XO, NA 1.42), using pulsed excitation lasers at 640 nm and a pulsed STED laser operating at 775 nm and gated detection with avalanche photodiode element detectors, where acquisition operations were controlled by Lightbox Software (Abberior Instruments GmbH). Some 2D STED images were also taken with an abberior STEDYCON with an inverted IX83 microscope (Olympus), a 100x oil objective (Olympus UPLXAPO100XO, NA 1.45), using pulsed excitation lasers at 640 nm and a pulsed STED laser operating at 775 nm, continuous autofocus and gated detection with avalanche photodiode element detectors, where the acquisition operations were controlled by STEDYCON Software (abberior Instruments), and images were deconvolved using Huygens deconvolution software.

Microscopic images shown are maximum projections or (where indicated) single plane images. All processing and measurements were done in Fiji (***Schindelin et al., 2012***) using the plug-ins NeuronJ for dendrite length measurements.

S2 cell culture, immunoprecipitation, and Western blots

S2R+ cells (DGRC) were thawed and expanded from frozen Mycoplasma-tested (with DAPI) stocks. Appropriate pUAST plasmids (Rab11::GFP (wt or S25N), Msps^{FLAG}, GFP::Patronin, myc::SRR27-32) were cotransfected with Actin5C-GAL4 as described (***Herzmann et al., 2017***). After 72 hr, cells were harvested in ice-cold PBS, and lysed in cold lysis buffer (100 mM NaCl, 5 mM $MgCl_2$, 50 mM Tris/HCl pH 7.6, 5% glycerol, 1% Triton X-100, 1x complete protease inhibitor). Cleared lysates were incubated with anti-FLAG beads (Sigma A-2220) or with rabbit anti-GFP antibodies (Invitrogen A11222) bound to protein A sepharose (GE Healthcare 17-5280-01) for 2 hr. After three washes with lysis buffer, bound proteins were eluted in SDS sample buffer. Samples were run on 8% gels and blotted with

JL-8 anti-GFP (Clontech, 1:1000), FLAG M2 (Sigma F3165, 1:5000), or myc 9E10 (in house, 1:50) antibodies. Bands were visualized on an Amersham Imager 680.

Quantification and statistical analyses

Phenotypic penetrance was assessed by counting the number of neurons with dendrites still attached to the soma. Here, significance was determined using a categorical two-tailed Fisher's exact test. Length of unpruned dendrites were measured using the Fiji NeuronJ plugin and compared using the Wilcoxon Mann–Whitney test. The number of dendritic kin::lacZ puncta was determined manually and compared using the Wilcoxon Mann–Whitney test. EB1 comet orientation was assessed using a categorical two-tailed Fisher's exact test, and a Mann–Whitney test was used to compare comet speed. In order to quantify Shot or EB1 dendrite tip localization, intensity profiles of the distal 10 µm of each dendrite were averaged. The resulting curves were then sectioned into 2 µm segments, and data points from the individual intensity profiles for each segment were pooled and used for statistical comparisons between genotypes using the Mann–Whitney test. To compare microtubule density, average cherry-tubulin fluorescence intensities along dendrites were normalized against cherry-tubulin fluorescence in the soma and compared using a Student's *t*-test. Presynapse numbers were determined as described (***Frommeyer et al., 2026***). Two-sample *t*-tests were performed in Excel; all other tests were performed using Prism 10 software or online (***Marx et al., 2016***). Where necessary, data were corrected for multiple comparisons using Bennett's test. All datasets were taken from multiple crosses over several days and are therefore biological replicates.

Acknowledgements

We thank T Zobel and S Weischer at the Münster Imaging Network for expert advice on superresolution microscopy, D Luchtman (abberior), S Volkery and Nils Kirschnick (BioOptics facility, MPI for Molecular Biomedicine) for help with 2D and 3D STED, A Prokop, G Tavosanis, J Wildonger, D Nashchekin, S Sigrist, the Bloomington, VDRC, and Kyoto stock centers, and Addgene for fly lines and reagents. We thank R Hube for technical help in the initial stages of the project, T Klein-Höing for help with cloning, and A Ziegler for advice on early larval c4da neuron imaging. MD, NS, SMF, and NW are members of the CiM IMPRS and CRC1348 graduate schools, respectively. This work was supported by DFG grants RU1673/4-1, RU1673/6-1, and RU1673/10-1 to SR. The authors declare no competing financial interests. Requests for UAS-EB1::mScarlet3 should be directed to Melissa Rolls (mur22@psu.edu). All newly generated reagents will be available upon request from SR.

Additional information

Funding

Funder	Grant reference number	Author
German Research Foundation	RU1673/4-1	Sebastian Rumpf
German Research Foundation	RU1673/6-1	Sebastian Rumpf
German Research Foundation	RU1673/10-1	Sebastian Rumpf

The funders had no role in study design, data collection, and interpretation, or the decision to submit the work for publication.

Author contributions

Matthew Davies, Conceptualization, Data curation, Formal analysis, Investigation, Methodology; Neeraja Sanal, Neele Wolterhoff, Ulrike Gigengack, Samuel M Frommeyer, Investigation; Yitao Shen, Ines Hahn, Resources; Sebastian Rumpf, Conceptualization, Data curation, Formal analysis, Supervision, Funding acquisition, Writing – original draft, Writing – review and editing

Author ORCIDs
Matthew Davies https://orcid.org/0009-0001-8229-4107
Neeraja Sanal https://orcid.org/0009-0001-8703-5956
Neele Wolterhoff https://orcid.org/0000-0001-7222-2866
Yitao Shen https://orcid.org/0000-0001-7956-8237
Samuel M Frommeyer https://orcid.org/0009-0005-5445-1223
Ines Hahn https://orcid.org/0000-0001-7703-8160
Sebastian Rumpf https://orcid.org/0000-0002-7128-2645

Peer review material
Version of Record:
Reviewer #1 (Public review): https://doi.org/10.7554/eLife.108055.3.sa1
Reviewer #2 (Public review): https://doi.org/10.7554/eLife.108055.3.sa2
Author response https://doi.org/10.7554/eLife.108055.3.sa3

Reviewed preprint v2
Reviewer #1 (Public review): https://doi.org/10.7554/eLife.108055.2.sa2
Reviewer #2 (Public review): https://doi.org/10.7554/eLife.108055.2.sa1
Author response: https://doi.org/10.7554/eLife.108055.2.sa0
eLife Assessment https://doi.org/10.7554/eLife.108055.2.sa3

Reviewed preprint v1
Reviewer #1 (Public review): https://doi.org/10.7554/eLife.108055.1.sa1
Reviewer #2 (Public review): https://doi.org/10.7554/eLife.108055.1.sa0
Author response: https://doi.org/10.7554/eLife.108055.1.sa3
eLife Assessment https://doi.org/10.7554/eLife.108055.1.sa2

Additional files

Supplementary files

MDAR checklist

Data availability

Microscopy data generated in this study as well as Excel sheets with the corresponding analyses have been made available at the European BioImage Archive under https://doi.org/10.6019/S-BIAD4199, and raw data for Western blots have been posted as source files with the corresponding figures.

The following dataset was generated:

Author(s)	Year	Dataset title	Dataset URL	Database and Identifier
Davies M, Wendt J, Rumpf S	2026	Spectraplakin is required for dendritic microtubule organization via a tip-based mechanism	https://doi.org/10.6019/S-BIAD4199	EBI, 10.6019/S-BIAD4199

References

Akhmanova A, Kapitein LC. 2022. Mechanisms of microtubule organization in differentiated animal cells. *Nature Reviews Molecular Cell Biology* **23**:541–558. DOI: https://doi.org/10.1038/s41580-022-00473-y, PMID: 35383336

Alves-Silva J, Sánchez-Soriano N, Beaven R, Klein M, Parkin J, Millard TH, Bellen HJ, Venken KJT, Ballestrem C, Kammerer RA, Prokop A. 2012. Spectraplakins promote microtubule-mediated axonal growth by functioning as structural microtubule-associated proteins and EB1-dependent +TIPs (tip interacting proteins). *The Journal of Neuroscience* **32**:9143–9158. DOI: https://doi.org/10.1523/JNEUROSCI.0416-12.2012, PMID: 22764224

An J, Imasaki T, Narita A, Niwa S, Sasaki R, Makino T, Nitta R, Kikkawa M. 2025. Dimerization of GAS2 mediates crosslinking of microtubules and F-actin. *The EMBO Journal* **44**:2997–3024. DOI: https://doi.org/10.1038/s44318-025-00415-2, PMID: 40169809

Applewhite DA, Grode KD, Duncan MC, Rogers SL. 2013. The actin-microtubule cross-linking activity of Drosophila Short stop is regulated by intramolecular inhibition. *Molecular Biology of the Cell* **24**:2885–2893. DOI: https://doi.org/10.1091/mbc.E12-11-0798, PMID: 23885120

Arthur AL, Yang SZ, Abellaneda AM, Wildonger J. 2015. Dendrite arborization requires the dynein cofactor NudE. *Journal of Cell Science* **128**:2191–2201. DOI: https://doi.org/10.1242/jcs.170316, PMID: 25908857

Clark IE, Jan LY, Jan YN. 1997. Reciprocal localization of Nod and kinesin fusion proteins indicates microtubule polarity in the *Drosophila* oocyte, epithelium, neuron and muscle. *Development* **124**:461–470. DOI: https://doi.org/10.1242/dev.124.2.461, PMID: 9053322

Dekker J, Schot R, Aldinger KA, Everman DB, Washington C, Jones JR, Sullivan JA, Spillmann RC, Shashi V, Vitobello A, Denommé-Pichon A-S, Mosca-Boidron A-L, Perrin L, Auvin S, Zaki MS, Gleeson JG, Meave N, Wallace C, Nambot S, Delanne J, et al. 2025. A clinical and genotype-phenotype analysis of MACF1 variants. *American Journal of Human Genetics* **112**:2363–2380. DOI: https://doi.org/10.1016/j.ajhg.2025.08.010, PMID: 40925378

Dietzl G, Chen D, Schnorrer F, Su KC, Barinova Y, Fellner M, Gasser B, Kinsey K, Oppel S, Scheiblauer S, Couto A, Marra V, Keleman K, Dickson BJ. 2007. A genome-wide transgenic RNAi library for conditional gene inactivation in Drosophila. *Nature* **448**:151–156. DOI: https://doi.org/10.1038/nature05954, PMID: 17625558

Feng C, Thyagarajan P, Shorey M, Seebold DY, Weiner AT, Albertson RM, Rao KS, Sagasti A, Goetschius DJ, Rolls MM. 2019. Patronin-mediated minus end growth is required for dendritic microtubule polarity. *The Journal of Cell Biology* **218**:2309–2328. DOI: https://doi.org/10.1083/jcb.201810155, PMID: 31076454

Frommeyer SM, Gigengack U, Rode S, Davies M, Wolterhoff N, Rumpf S. 2026. The mRNA export factor UAP56 is required for dendrite and synapse pruning via actin regulation in *Drosophila*. *Journal of Cell Science* **139**:jcs264770. DOI: https://doi.org/10.1242/jcs.264770, PMID: 41958408

Furusawa K, Emoto K. 2021. Spatiotemporal regulation of developmental neurite pruning: Molecular and cellular insights from *Drosophila* models. *Neuroscience Research* **167**:54–63. DOI: https://doi.org/10.1016/j.neures.2020.11.010, PMID: 33309868

Furusawa K, Ishii K, Tsuji M, Tokumitsu N, Hasegawa E, Emoto K. 2023. Presynaptic Ube3a E3 ligase promotes synapse elimination through down-regulation of BMP signaling. *Science* **381**:1197–1205. DOI: https://doi.org/10.1126/science.ade8978, PMID: 37708280

Gadella TJ, van Weeren L, Stouthamer J, Hink MA, Wolters AHG, Giepmans BNG, Aumonier S, Dupuy J, Royant A. 2023. mScarlet3: a brilliant and fast-maturing red fluorescent protein. *Nature Methods* **20**:541–545. DOI: https://doi.org/10.1038/s41592-023-01809-y, PMID: 36973546

Grintsevich EE, Ge P, Sawaya MR, Yesilyurt HG, Terman JR, Zhou ZH, Reisler E. 2017. Catastrophic disassembly of actin filaments via Mical-mediated oxidation. *Nature Communications* **8**:2183. DOI: https://doi.org/10.1038/s41467-017-02357-8, PMID: 29259197

Grueber WB, Ye B, Yang CH, Younger S, Borden K, Jan LY, Jan YN. 2007. Projections of *Drosophila* multidendritic neurons in the central nervous system: links with peripheral dendrite morphology. *Development* **134**:55–64. DOI: https://doi.org/10.1242/dev.02666, PMID: 17164414

Hahn I, Voelzmann A, Parkin J, Fülle JB, Slater PG, Lowery LA, Sanchez-Soriano N, Prokop A. 2021. Tau, XMAP215/Msps and Eb1 co-operate interdependently to regulate microtubule polymerisation and bundle formation in axons. *PLOS Genetics* **17**:e1009647. DOI: https://doi.org/10.1371/journal.pgen.1009647, PMID: 34228717

Harterink M, Edwards SL, de Haan B, Yau KW, van den Heuvel S, Kapitein LC, Miller KG, Hoogenraad CC. 2018. Local microtubule organization promotes cargo transport in *C. elegans* dendrites. *Journal of Cell Science* **131**:jcs223107. DOI: https://doi.org/10.1242/jcs.223107, PMID: 30254025

He L, Kooistra R, Das R, Oudejans E, van Leen E, Ziegler J, Portegies S, de Haan B, van Regteren Altena A, Stucchi R, Altelaar AM, Wieser S, Krieg M, Hoogenraad CC, Harterink M. 2020. Cortical anchoring of the microtubule cytoskeleton is essential for neuron polarity. *eLife* **9**:e55111. DOI: https://doi.org/10.7554/eLife.55111, PMID: 32293562

He L, van Beem L, Snel B, Hoogenraad CC, Harterink M. 2022. PTRN-1 (CAMSAP) and NOCA-2 (NINEIN) are required for microtubule polarity in *Caenorhabditis elegans* dendrites. *PLOS Biology* **20**:e3001855. DOI: https://doi.org/10.1371/journal.pbio.3001855, PMID: 36395330

Herzmann S, Krumkamp R, Rode S, Kintrup C, Rumpf S. 2017. PAR-1 promotes microtubule breakdown during dendrite pruning in *Drosophila*. *The EMBO Journal* **36**:1981–1991. DOI: https://doi.org/10.15252/embj.201695890, PMID: 28554895

Herzmann S, Götzelmann I, Reekers LF, Rumpf S. 2018. Spatial regulation of microtubule disruption during dendrite pruning in *Drosophila*. *Development* **145**:dev156950. DOI: https://doi.org/10.1242/dev.156950, PMID: 29712642

Hung RJ, Yazdani U, Yoon J, Wu H, Yang T, Gupta N, Huang Z, van Berkel WJH, Terman JR. 2010. Mical links semaphorins to F-actin disassembly. *Nature* **463**:823–827. DOI: https://doi.org/10.1038/nature08724, PMID: 20148037

Ka M, Kim WY. 2016. Microtubule-actin crosslinking factor 1 Is required for dendritic arborization and axon outgrowth in the developing brain. *Molecular Neurobiology* **53**:6018–6032. DOI: https://doi.org/10.1007/s12035-015-9508-4, PMID: 26526844

Khanal I, Elbediwy A, Diaz de la Loza MDC, Fletcher GC, Thompson BJ. 2016. Shot and Patronin polarise microtubules to direct membrane traffic and biogenesis of microvilli in epithelia. *Journal of Cell Science* **129**:2651–2659. DOI: https://doi.org/10.1242/jcs.189076, PMID: 27231092

Kirilly D, Gu Y, Huang Y, Wu Z, Bashirullah A, Low BC, Kolodkin AL, Wang H, Yu F. 2009. A genetic pathway composed of Sox14 and Mical governs severing of dendrites during pruning. *Nature Neuroscience* **12**:1497–1505. DOI: https://doi.org/10.1038/nn.2415, PMID: 19881505

Kolodziej PA, Jan LY, Jan YN. 1995. Mutations that affect the length, fasciculation, or ventral orientation of specific sensory axons in the *Drosophila* embryo. *Neuron* **15**:273–286. DOI: https://doi.org/10.1016/0896-6273(95)90033-0, PMID: 7646885

Krämer R, Rode S, Rumpf S. 2019. Rab11 is required for neurite pruning and developmental membrane protein degradation in Drosophila sensory neurons. *Developmental Biology* **451**:68–78. DOI: https://doi.org/10.1016/j.ydbio.2019.03.003, PMID: 30871987

Krämer R, Wolterhoff N, Galic M, Rumpf S. 2023. Developmental pruning of sensory neurites by mechanical tearing in *Drosophila*. *The Journal of Cell Biology* **222**:222. DOI: https://doi.org/10.1083/jcb.202205004, PMID: 36648440

Kuo CT, Jan LY, Jan YN. 2005. Dendrite-specific remodeling of *Drosophila* sensory neurons requires matrix metalloproteases, ubiquitin-proteasome, and ecdysone signaling. *PNAS* **102**:15230–15235. DOI: https://doi.org/10.1073/pnas.0507393102, PMID: 16210248

Lee S, Kolodziej PA. 2002. Short Stop provides an essential link between F-actin and microtubules during axon extension. *Development* **129**:1195–1204. DOI: https://doi.org/10.1242/dev.129.5.1195, PMID: 11874915

Liang X, Kokes M, Fetter RD, Sallee MD, Moore AW, Feldman JL, Shen K. 2020. Growth cone-localized microtubule organizing center establishes microtubule orientation in dendrites. *eLife* **9**:e56547. DOI: https://doi.org/10.7554/eLife.56547, PMID: 32657271

Liang X, Agulto R, Eichel K, Taylor CA, Paat VA, Deng H, Ori-McKenney K, Shen K. 2025. CRMP/UNC-33 maintains neuronal microtubule arrays by promoting individual microtubule rescue. *Current Biology* **35**:734–745. DOI: https://doi.org/10.1016/j.cub.2024.12.030, PMID: 39842439

Lin T, Kao HH, Chou CH, Chou CY, Liao YC, Lee HH. 2020. Rab11 activation by Ik2 kinase is required for dendrite pruning in Drosophila sensory neurons. *PLOS Genetics* **16**:e1008626. DOI: https://doi.org/10.1371/journal.pgen.1008626, PMID: 32059017

Marx A, Backes C, Meese E, Lenhof H-P, Keller A. 2016. EDISON-WMW: exact dynamic programing solution of the Wilcoxon–Mann–Whitney test. *Genomics, Proteomics & Bioinformatics* **14**:55–61. DOI: https://doi.org/10.1016/j.gpb.2015.11.004

Marzano M, Herzmann S, Elsbroek L, Sanal N, Tarbashevich K, Raz E, Krahn MP, Rumpf S. 2021. AMPK adapts metabolism to developmental energy requirement during dendrite pruning in Drosophila. *Cell Reports* **37**:110024. DOI: https://doi.org/10.1016/j.celrep.2021.110024, PMID: 34788610

Matsubara D, Horiuchi SY, Shimono K, Usui T, Uemura T. 2011. The seven-pass transmembrane cadherin Flamingo controls dendritic self-avoidance via its binding to a LIM domain protein, Espinas, in Drosophila sensory neurons. *Genes & Development* **25**:1982–1996. DOI: https://doi.org/10.1101/gad.16531611, PMID: 21937715

Mattie FJ, Stackpole MM, Stone MC, Clippard JR, Rudnick DA, Qiu Y, Tao J, Allender DL, Parmar M, Rolls MM. 2010. Directed microtubule growth, +TIPs, and kinesin-2 are required for uniform microtubule polarity in dendrites. *Current Biology* **20**:2169–2177. DOI: https://doi.org/10.1016/j.cub.2010.11.050, PMID: 21145742

Mukherjee A, Brooks PS, Bernard F, Guichet A, Conduit PT. 2020. Microtubules originate asymmetrically at the somatic golgi and are guided via Kinesin2 to maintain polarity within neurons. *eLife* **9**:e58943. DOI: https://doi.org/10.7554/eLife.58943, PMID: 32657758

Nashchekin D, Fernandes AR, St Johnston D. 2016. Patronin/shot cortical foci assemble the noncentrosomal microtubule array that specifies the *Drosophila* anterior-posterior axis. *Developmental Cell* **38**:61–72. DOI: https://doi.org/10.1016/j.devcel.2016.06.010, PMID: 27404359

Nashchekin D, Squires I, Prokop A, St Johnston D. 2024. The Shot CH1 domain recognises a distinct form of F-actin during Drosophila oocyte determination. *Development* **151**:151. DOI: https://doi.org/10.1242/dev.202370, PMID: 38564309

Nguyen MM, Stone MC, Rolls MM. 2011. Microtubules are organized independently of the centrosome in Drosophila neurons. *Neural Development* **6**:38. DOI: https://doi.org/10.1186/1749-8104-6-38, PMID: 22145670

Nguyen MM, McCracken CJ, Milner ES, Goetschius DJ, Weiner AT, Long MK, Michael NL, Munro S, Rolls MM. 2014. Γ-tubulin controls neuronal microtubule polarity independently of Golgi outposts. *Molecular Biology of the Cell* **25**:2039–2050. DOI: https://doi.org/10.1091/mbc.E13-09-0515, PMID: 24807906

Ning W, Yu Y, Xu H, Liu X, Wang D, Wang J, Wang Y, Meng W. 2016. The CAMSAP3-ACF7 complex couples noncentrosomal microtubules with actin filaments to coordinate their dynamics. *Developmental Cell* **39**:61–74. DOI: https://doi.org/10.1016/j.devcel.2016.09.003, PMID: 27693509

Noordstra I, Liu Q, Nijenhuis W, Hua S, Jiang K, Baars M, Remmelzwaal S, Martin M, Kapitein LC, Akhmanova A. 2016. Control of apico-basal epithelial polarity by the microtubule minus-end-binding protein CAMSAP3 and spectraplakin ACF7. *Journal of Cell Science* **129**:4278–4288. DOI: https://doi.org/10.1242/jcs.194878, PMID: 27802168

Okenve-Ramos P, Gosling R, Chojnowska-Monga M, Gupta K, Shields S, Alhadyian H, Collie C, Gregory E, Sanchez-Soriano N. 2024. Neuronal ageing is promoted by the decay of the microtubule cytoskeleton. *PLOS Biology* **22**:e3002504. DOI: https://doi.org/10.1371/journal.pbio.3002504, PMID: 38478582

Ori-McKenney KM, Jan LY, Jan YN. 2012. Golgi outposts shape dendrite morphology by functioning as sites of acentrosomal microtubule nucleation in neurons. *Neuron* **76**:921–930. DOI: https://doi.org/10.1016/j.neuron.2012.10.008, PMID: 23217741

Rajan S, Terman JR, Reisler E. 2023. MICAL-mediated oxidation of actin and its effects on cytoskeletal and cellular dynamics. *Frontiers in Cell and Developmental Biology* **11**:1124202. DOI: https://doi.org/10.3389/fcell.2023.1124202, PMID: 36875759

Rode S, Ohm H, Anhäuser L, Wagner M, Rosing M, Deng X, Sin O, Leidel SA, Storkebaum E, Rentmeister A, Zhu S, Rumpf S. 2018. Differential requirement for translation initiation factor pathways during ecdysone-dependent neuronal remodeling in *Drosophila*. *Cell Reports* **24**:2287–2299. DOI: https://doi.org/10.1016/j.celrep.2018.07.074, PMID: 30157424

Rolls MM, Satoh D, Clyne PJ, Henner AL, Uemura T, Doe CQ. 2007. Polarity and intracellular compartmentalization of *Drosophila* neurons. *Neural Development* **2**:7. DOI: https://doi.org/10.1186/1749-8104-2-7, PMID: 17470283

Rui M, Ng KS, Tang Q, Bu S, Yu F. 2020. Protein phosphatase PP2A regulates microtubule orientation and dendrite pruning in Drosophila. *EMBO Reports* **21**:e48843. DOI: https://doi.org/10.15252/embr.201948843, PMID: 32187821

Rumpf S, Rode S, Herzmann S, Krumkamp R. 2017. Mechanisms of Neurite Pruning. *E-Neuroforum* **23**:19–25. DOI: https://doi.org/10.1515/nf-2016-A105

Rumpf S, Wolterhoff N, Herzmann S. 2019. Functions of microtubule disassembly during neurite pruning. *Trends in Cell Biology* **29**:291–297. DOI: https://doi.org/10.1016/j.tcb.2019.01.002, PMID: 30683460

Sanal N, Keding L, Gigengack U, Michalke E, Rumpf S. 2023. TORC1 regulation of dendrite regrowth after pruning is linked to actin and exocytosis. *PLOS Genetics* **19**:e1010526. DOI: https://doi.org/10.1371/journal.pgen.1010526, PMID: 37167328

Sanchez AD, Branon TC, Cote LE, Papagiannakis A, Liang X, Pickett MA, Shen K, Jacobs-Wagner C, Ting AY, Feldman JL. 2021. Proximity labeling reveals non-centrosomal microtubule-organizing center components required for microtubule growth and localization. *Current Biology* **31**:3586–3600. DOI: https://doi.org/10.1016/j.cub.2021.06.021

Schindelin J, Arganda-Carreras I, Frise E, Kaynig V, Longair M, Pietzsch T, Preibisch S, Rueden C, Saalfeld S, Schmid B, Tinevez JY, White DJ, Hartenstein V, Eliceiri K, Tomancak P, Cardona A. 2012. Fiji: an open-source platform for biological-image analysis. *Nature Methods* **9**:676–682. DOI: https://doi.org/10.1038/nmeth.2019, PMID: 22743772

Slep KC, Rogers SL, Elliott SL, Ohkura H, Kolodziej PA, Vale RD. 2005. Structural determinants for EB1-mediated recruitment of APC and spectraplakins to the microtubule plus end. *The Journal of Cell Biology* **168**:587–598. DOI: https://doi.org/10.1083/jcb.200410114, PMID: 15699215

Sun T, Song Y, Dai J, Mao D, Ma M, Ni JQ, Liang X, Pastor-Pareja JC. 2019. Spectraplakin shot maintains perinuclear microtubule organization in *Drosophila* polyploid cells. *Developmental Cell* **49**:731–747. DOI: https://doi.org/10.1016/j.devcel.2019.03.027, PMID: 31006649

Tang Q, Rui M, Bu S, Wang Y, Chew LY, Yu F. 2020. A microtubule polymerase is required for microtubule orientation and dendrite pruning in Drosophila. *The EMBO Journal* **39**:e103549. DOI: https://doi.org/10.15252/embj.2019103549, PMID: 32267553

Terman JR, Mao T, Pasterkamp RJ, Yu HH, Kolodkin AL. 2002. MICALs, a family of conserved flavoprotein oxidoreductases, function in plexin-mediated axonal repulsion. *Cell* **109**:887–900. DOI: https://doi.org/10.1016/s0092-8674(02)00794-8, PMID: 12110185

Villars A, Matamoro-Vidal A, Levillayer F, Levayer R. 2022. Microtubule disassembly by caspases is an important rate-limiting step of cell extrusion. *Nature Communications* **13**:3632. DOI: https://doi.org/10.1038/s41467-022-31266-8, PMID: 35752632

Voelzmann A, Liew YT, Qu Y, Hahn I, Melero C, Sánchez-Soriano N, Prokop A. 2017. Drosophila Short stop as a paradigm for the role and regulation of spectraplakins. *Seminars in Cell & Developmental Biology* **69**:40–57. DOI: https://doi.org/10.1016/j.semcdb.2017.05.019, PMID: 28579450

Voelzmann A, Nuhu-Soso L, Roof AE, Patel S, Bennett H, Adamson A, Evans GJO, Bentley M, Hahn I. 2026. GSK-3β coordinates axonal microtubule organization through Shot and Tau. *PNAS* **123**:e2516746123. DOI: https://doi.org/10.1073/pnas.2516746123, PMID: 41701831

Wang Y, Rui M, Tang Q, Bu S, Yu F. 2019. Patronin governs minus-end-out orientation of dendritic microtubules to promote dendrite pruning in *Drosophila*. *eLife* **8**:e39964. DOI: https://doi.org/10.7554/eLife.39964, PMID: 30920370

Weiner AT, Seebold DY, Torres-Gutierrez P, Folker C, Swope RD, Kothe GO, Stoltz JG, Zalenski MK, Kozlowski C, Barbera DJ, Patel MA, Thyagarajan P, Shorey M, Nye DMR, Keegan M, Behari K, Song S, Axelrod JD, Rolls MM. 2020. Endosomal Wnt signaling proteins control microtubule nucleation in dendrites. *PLOS Biology* **18**:e3000647. DOI: https://doi.org/10.1371/journal.pbio.3000647, PMID: 32163403

Williams DW, Truman JW. 2005. Cellular mechanisms of dendrite pruning in *Drosophila*: insights from in vivo time-lapse of remodeling dendritic arborizing sensory neurons. *Development* **132**:3631–3642. DOI: https://doi.org/10.1242/dev.01928, PMID: 16033801

Wolterhoff N, Gigengack U, Rumpf S. 2020. PP2A phosphatase is required for dendrite pruning via actin regulation in *Drosophila*. *EMBO Reports* **21**:e48870. DOI: https://doi.org/10.15252/embr.201948870, PMID: 32207238

Yalgin C, Ebrahimi S, Delandre C, Yoong LF, Akimoto S, Tran H, Amikura R, Spokony R, Torben-Nielsen B, White KP, Moore AW. 2015. Centrosomin represses dendrite branching by orienting microtubule nucleation. *Nature Neuroscience* **18**:1437–1445. DOI: https://doi.org/10.1038/nn.4099, PMID: 26322925

Yoong LF, Lim HK, Tran H, Lackner S, Zheng Z, Hong P, Moore AW. 2020. Atypical myosin tunes dendrite arbor subdivision. *Neuron* **106**:452–467. DOI: https://doi.org/10.1016/j.neuron.2020.02.002, PMID: 32155441

Zheng Y, Wildonger J, Ye B, Zhang Y, Kita A, Younger SH, Zimmerman S, Jan LY, Jan YN. 2008. Dynein is required for polarized dendritic transport and uniform microtubule orientation in axons. *Nature Cell Biology* **10**:1172–1180. DOI: https://doi.org/10.1038/ncb1777, PMID: 18758451